

IMAGE PROCESSING BASED HAPTIC GUIDANCE SYSTEM FOR VISUALLY
IMPAIRED RUNNERS

by

Oğuz Kayhan

B.S., Mechanical Engineering, Boğaziçi University, 2017

Submitted to the Institute for Graduate Studies in
Science and Engineering in partial fulfillment of
the requirements for the degree of
Master of Science

Graduate Program in Mechanical Engineering
Boğaziçi University

2021

ACKNOWLEDGEMENTS

First and foremost, I would like to express my sincere gratitude to my advisor, Assoc. Prof. Evren Samur, for his continuous support during my both bachelor and master study. I am grateful to him for sharing his valuable experiences helping me to accomplish of this work and giving me the opportunity to study with him.

Secondly, I am grateful to Prof. Çetin Yılmaz, Prof. Hakan Ertürk and Assoc. Prof. Hande Sart to initiate my study. I would like to thank Cenk Taşkın, Emre Aslan, Emre Yiğitbaşı and all the people who had been worked in the preliminary study of this project. Also, I would like to pay my special regards to Engin Yılmaz and people in Boğaziçi University Visually Impaired Technology and Education Center (GETEM), for their interest to my study and supporting me through their advises. I wish the device I developed during this study will be used by them one day and reach its aim.

Most especially, I would like to express my gratitude to my family, Cemile Kayhan, Ekrem Kayhan and Ceren Kayhan for encouraging me with their love. Also, I would like to express my special thanks to my lovely wife, Asude Pelin Kayhan, for her endless support to complete this study, encouragement, patience and also not losing her faith in me during my academic life. Also, I would like to thank her for her assistance to my study by her academic experiences and valuable contribution on the design of the device to make it more usable.

Last but not the least, I am also grateful to my extended family, all my friends in our little gang and our laboratory group, for their encouragement and expanding my horizon. But most especially, I'm grateful to my best man Sergen Haydn for his contribution to my study, his valuable friendship and for his trust and support whenever I needed.

ABSTRACT

IMAGE PROCESSING BASED HAPTIC GUIDANCE SYSTEM FOR VISUALLY IMPAIRED RUNNERS

People with disabilities face too many problems in their daily lives. The defeat of visual perception seriously confines a person's daily life and activities. For example, visually impaired people have difficulty to move around in unknown environment because they cannot determine exact object locations in their surroundings. It is even more challenging to do sports such as running on a track lanes. In this study, a wearable haptic guidance system has been developed which can help visually impaired individuals to navigate on a lane of athletic track. The system is based on image processing, and thus, includes a micro-controller, servo motors, a camera and a battery. The camera is used to feed lane detection and steering angle calculation pipeline. The skin stretch method is used to transfer calculated steering angles to the user. In order to evaluate the proposed algorithm and the feedback system, several tests have been conducted. According to the experiment results, the algorithm can detect lanes with an accuracy of 86.5 %, and the feedback system helps the user distinguish different feedback directions and magnitudes with an accuracy of 88.3 %. Considering these results, we can conclude that the designed haptic system is a promising tool for visually impaired runners navigating in an athletic track.

ÖZET

GÖRME ENGELLİ KOŞUCULAR İÇİN GÖRÜNTÜ İŞLEME VE DOKUNSA GERİ BESLEME TABANLI YÖNLENDİRME SİSTEMİ

Engelli bireyler günlük yaşantılarında çok fazla engelle karşılaşılıyorlar. Görsel algının yitirilmesi ya da azalması, bir kişinin günlük yaşamını ve aktivitelerini ciddi şekilde sınırlar. Örnek vermek gerekirse, görme engelli kişiler, çevrelerindeki nesnelere yerini tam olarak belirleyemedikleri için bilinmeyen ortamlarda hareket etmekte zorluk çekerler. Normal yaşantılarına nazaran spor aktivitelerinde bulunmak onlar için daha da zorlayıcıdır. Bu çalışmada, atletik bir parkur içerisinde koşan görme engelli bireyleri yönlendirebilen giyilebilir haptik rehberlik sistemi geliştirilmiştir. Sistem görüntü işlemeye tabanlıdır ve içeriğinde mikro denetleyici, servo motorlar, bir kamera ve bir güç kaynağı bulundurulur. Kamera, şerit algılama ve dönüş açısı hesaplama algoritmalarını beslemek için kullanılmaktadır. Hesaplanan dönüş açıları kullanıcıya aktarmak için deri çekme yöntemi kullanılmaktadır. Tasarlanan cihaz üretildikten sonra, algoritma ve geri bildirim sistemi performansını değerlendirmek için çeşitli testler yapılmıştır. Deney sonuçlarına göre, geliştirilen algoritma şeritleri % 86,5 doğrulukla algılamaktadır, ve geri bildirim sistemi kullanıcının farklı geri bildirimlerin yönünü ve büyüklüğünü % 88,3 doğrulukla ayırt etmesine yardımcı olmaktadır. Test sonuçları göz önüne alındığında, tasarlanan haptik sistemin görme engelli bireylerin tek başlarına koşmalarına yardımcı olacağı öngörülmektedir.

TABLE OF CONTENTS

ACKNOWLEDGEMENTS	i
ACKNOWLEDGEMENTS	ii
ABSTRACT	iii
ÖZET	iv
LIST OF FIGURES	vii
LIST OF TABLES	xi
LIST OF SYMBOLS	xii
LIST OF ACRONYMS/ABBREVIATIONS	xiii
1. INTRODUCTION	1
1.1. Motivation	1
1.2. Aims	2
1.3. Literature Review	3
1.3.1. Navigation Systems for Visually Impaired Persons based on Smart White Canes	4
1.3.2. Wearable Navigation System	6
1.3.3. Navigation Systems for Visually Impaired Athletes	13
2. MATERIALS AND METHODS	15
2.1. System Overview	15
2.2. Lane Detection Algorithm	16
2.2.1. General Detection Pipeline	16
2.2.2. Image Spaces and Color Filters	17
2.2.3. Gradient Filters	20
2.2.4. Perspective Transform	24
2.2.5. Sliding Window Algorithm and Polynomial Fits	25
2.2.6. Curvature Calculation and Steering	26
2.2.6.1. Pixel to meter transformation	26
2.3. Servo Control	28
2.4. Haptic Feedback System Design and Working Principle	30

2.5. Skin Stretch Physical Modelling and Calculations	32
3. EXPERIMENTAL METHODS	35
3.1. Lane Detection and Steering Calculation Tests	35
3.2. Skin Stretch Feedback Performance Tests	36
3.2.1. Static Tests	36
3.2.2. Pre-recorded Test	38
3.2.3. Real-time Test	38
4. RESULTS and DISCUSSION	39
4.1. Algorithm Performance	39
4.1.1. Lane Detection Performance	39
4.1.2. Steering Angle Calculation Performance	41
4.2. Haptic Feedback Performance of System	46
4.2.1. Static Test Results	46
4.2.2. Pre-recorded Test Results	49
4.2.3. Real-time Test Results	51
5. CONCLUSION	54
5.1. Contributions and Originality	54
5.2. Future Work	55
REFERENCES	56
APPENDIX A: DATASHEET	62

LIST OF FIGURES

Figure 1.1.	A traditional white cane fitted with the smart system.	5
Figure 1.2.	Prototype of CNN based wearable assistive device	7
Figure 1.3.	Smart helmet system that can detects obstacles and transmits them to user via headphone	8
Figure 1.4.	Dual channel human machine interaction system prototype	9
Figure 1.5.	Tactile grid belt	10
Figure 1.6.	Sensor belt is located at bottom and haptic belt is located at top .	11
Figure 1.7.	Vibrotactile foam shoe insole design	12
Figure 1.8.	Waist type hanger reflex device and working principle	12
Figure 1.9.	Backside of the prototypic structure of the integrated navigation device. Consisting of light backpack (1), processing unit (2) and integrated vibration motors in the straps (3).	13
Figure 1.10.	EyeVista track detection and warning	14
Figure 2.1.	Prototype of the haptic guidance system.	15
Figure 2.2.	Lane detection pipeline.	16
Figure 2.3.	HLS and HSV color spaces representation.	17

Figure 2.4.	RGB-HLS-HSV view of specific frame.	18
Figure 2.5.	a)Unfiltered frame, b)Filtered with combined (S and L) channels.	20
Figure 2.6.	Horizontal gradient filter results.	22
Figure 2.7.	Vertical gradient filter results.	23
Figure 2.8.	Original frame and perspective transform result.	25
Figure 2.9.	Lane centre offset illustration.	27
Figure 2.10.	Steering angle calculation parameters of the reference point.	28
Figure 2.11.	Servo position for different signal width	29
Figure 2.12.	CAD model of prototype.	30
Figure 2.13.	Desired feedbacks of prototype.	31
Figure 2.14.	Illustration of skin-string analogy	33
Figure 2.15.	Required force and steering angle relation.	34
Figure 3.1.	Running track illustration.	35
Figure 3.2.	Static test estimation chart.	37
Figure 3.3.	Pre-recorded test response collection interface.	38

Figure 4.1.	Lane detection results. a) Turning part of track, b) Straight part of track.	40
Figure 4.2.	Steering angle results (Lane-1-CCW-5.5 km/h) vs desired steering angles.	42
Figure 4.3.	Steering angle results (Lane-3-CCW-5.5 km/h) vs desired steering angles.	42
Figure 4.4.	Steering angle results (Lane-5-CCW-5.5 km/h) vs desired steering angles.	42
Figure 4.5.	Steering angle results (Lane-1-CCW-6.6 km/h) vs desired steering angles.	43
Figure 4.6.	Steering angle results (Lane-3-CCW-6.6 km/h) vs desired steering angles.	43
Figure 4.7.	Steering angle results (Lane-5-CCW-6.6 km/h) vs desired steering angles.	43
Figure 4.8.	Steering angle results (Lane-1-CW-5.5 km/h) vs desired steering angles.	44
Figure 4.9.	Steering angle results (Lane-3-CW-5.5 km/h) vs desired steering angles.	44
Figure 4.10.	Steering angle results (Lane-5-CW-5.5 km/h) vs desired steering angles.	44

Figure 4.11. Steering angle results (Lane-1-CW-6.6 km/h) vs desired steering angles.	45
Figure 4.12. Steering angle results (Lane-3-CW-6.6 km/h) vs desired steering angles.	45
Figure 4.13. Steering angle results (Lane-5-CW-6.6 km/h) vs desired steering angles.	45
Figure 4.14. Confusion matrix of Test-1.	47
Figure 4.15. Confusion matrix of Test-2.	48
Figure 4.16. First pre-recorded test steering angle comparison.	49
Figure 4.17. Second pre-recorded test steering angle comparison.	50
Figure 4.18. Preparation and implementation phase of the real-time test.	51
Figure A.1. Servo motor datasheet.	62

LIST OF TABLES

Table 4.1.	Success rate of all video records.	39
Table 4.2.	Root mean square errors (RMSE) of the calculated steering angles for all running records.	46
Table 4.3.	Static test prediction accuracies of all subjects	47
Table 4.4.	RMSE of first and second pre-recorded tests.	51
Table 4.5.	Real-time test results of all subjects	52
Table 4.6.	Questionnaire results.	53

LIST OF SYMBOLS

B	Blue channel
F_r	Required force to stretch the skin
G	Green channel
H	Hue channel
k_s	Skin stiffness
L	Lightness channel
M	Perspective transformation matrix
R	Red channel
r_c	Radius of pulley which is attached to servo motor
R_{curve}	Radius of curvature
S	Saturation channel
S_x	Gradient approximation - Sobel filter in x direction
S_y	Gradient approximation - Sobel filter in y direction
S_{xy}	Gradient magnitude
V	Value channel
V_{max}	Maximum of R,G and B channels
V_{min}	Minimum of R,G and B channels
X_{cperpx}	Pixel to meter transformation coefficient for x direction
$x_{lane-centre}$	x axis position of lane centre
x_{left}	Second order polynomial for left lane
x_{right}	Second order polynomial for right lane
x_s	Amount of grasping strap movement
Y_{cperpy}	Pixel to meter transformation coefficient for y direction
δ_s	Amount of skin stretch
θ	Gradient direction
θ_s	Steering angle

LIST OF ACRONYMS/ABBREVIATIONS

API	Application Programming Interface
CW	Clockwise
CCW	Counter Clockwise
CNN	Convolutinal Neural Network
DC	Direct Current
ETA	Electronic Travel Aids
GPIO	General Purpose Input/Output
GPS	Global Positioning System
GSM	Global System for Mobile Communications
HALO	Haptic Alerts for Low-hanging Obstacles
HLS	Hue-Ligthness-Saturation
HSV	Hue-Saturation-Value
IMU	Inertial Measurement Unit
LIDAR	Laser Imaging Detection and Ranging
OpenCV	Open Source Computer Vision Library
PWM	Pulse Width Modulation
RFID	Radio Frequency Identification
RGB	Red-Green-Blue
RGB-D	Red-Green-Blue-Depth
RMSE	Root Mean Square Error
ROS	Robot Operating System
TOF	Time of Flight
USB	Universal Serial Bus
WHO	World Health Organization

1. INTRODUCTION

1.1. Motivation

Movement capability from one place to another is an important part of everyday life. Most people would admit that eyesight is a necessary part of safe navigation but would also have considerable difficulty in recognizing visual details for navigation. However, it is quite clear that vision is a key factor for safer and better navigation.

People with disabilities face too many problems in their daily lives. The defeat of visual perception seriously confines a person's daily life and activities. Visually impaired people may have difficulty to move around unknown environment because they cannot determine exact object locations in their surroundings. According to the research conducted by the World Health Organization (WHO) in 2014, it has been determined that there are 285 million visually impaired people in the world, 39 million of whom are blind and 246 million of whom have low vision [1] .

In recent years, it has been seen that there is a massive increase in the number of assistive technology study which improves the capacity of people with disabilities and encourages them to act independently in their lives. Assistive technology also supports severe visually impaired people in the world for their orientation and navigation in their regular activities [2].

These assistive technologies can be used in daily life or different activities which are not usual thing for everyday life. Doing sports, dancing, using a car can be listed as different activities. However, if someone try to create equal life for these people, all aspects of life should be considered. There are some works which targeted visually impaired people practicing sport activities such as, jogging and soft running [3]. Moreover, sport activities for impaired people are clearly stated at the article 30 of the Convention on the Rights of Persons with Disabilities [4].

Wearable devices possess a high potential for assistive applications for visually impaired as they contained a camera and feedback system for navigation. There are several works on wearable devices which are made for visually impaired athletes [2,5–7]. All of these devices include a camera for understanding the environment, and create instructions for athletes. However, critical difference between these devices arises in feedback mechanism for the user. After analyzing camera data, output can be transmitted to runner with different ways such as, auditory system, vibrotactile stimulation and skin stretch mechanism. Although all of these techniques have successfully implemented various haptic feedback mechanisms, which technique is more intuitive for visually impaired navigation is still an open question. Vibrational feedback has often been used as binary feedback. It has successful applications in giving alerts and navigating the user. However, when considering a proportional feedback, the vibrational feedback is not as useful as the skin stretch method. Since it will be more appropriate to navigate the visually impaired with proportional feedback, the skin stretch method will be a more intuitive choice.

Another improvement may be required for environmental monitoring because the running and walking activities of visually impaired people usually take place in outdoor conditions. Some variable conditions such as sunlight and shadows place a restriction on sensors performance which is needed to monitor environment. These variable outdoor environment conditions make wearable assistive device application more challenging. Assistive device users require constant inputs for their direction and speed. In order to get these constant inputs, environmental monitoring should work perfectly. Most of the studies in literature focused on classical machine vision techniques. However, a robust algorithm for all environmental conditions remains a challenge.

1.2. Aims

The purpose of this study is to design a system to help visually impaired individuals running on a lane of athletic track without the help of others. Preliminary version of the haptic feedback system has been designed by Taşkın et al. [8]. In this prelimi-

nary design, a mechanism was attached to a hat, and skin stretch feedback was given according to the desired input. Lane detection and obstacle detection algorithms were studied separately for the preliminary design. However, a robust prototype was not created in the previous study. In this thesis, a fully-functioning prototype is developed and presented.

The following aims were realized in this study:

Aim 1: To develop an image processing algorithm that can detect running lanes and calculates steering angle for navigation.

Aim 2: To design a haptic device that can guide the visually-impaired runners with respect to the image processing algorithm output. This device is designed as a feedback belt including electric motors and a touching pad that can be used for skin stretch feedback.

Aim 3 : To develop a robust prototype to merge the haptic feedback device with the algorithm, and perform user evaluation tests on a running track. Subjects are expected to intuitively navigate along the track with this prototype.

1.3. Literature Review

Visually impaired people encounter several unique challenges while navigating in unknown environments. Assistive technology studies have gained great importance in recent years and various devices have been introduced to make visually impaired life easier. Electronic travel aids (ETAs) are results of assistive technology studies, and these devices encourage visually impaired people to act equal in public. Detecting lane lines, obstacles on the ground or body level are quite critical for safe navigation. Environmental monitoring can be achieved through various sensors and cameras such as ultrasonic, laser range finder, LIDAR, depth, stereo, and RGB. Another important aspect for ETAs is type of feedback. There are two main feedback methods used in

assistive technology studies for visually impaired people that are audio feedback and haptic feedback. Audio feedback is given with earphone and speaker. Haptic feedback is usually provided with vibration and skin stretch. Vibrational feedback relies on a motion or force to be applied on the skin in order to trigger the mechanoreceptors on the skin [9]. This feedback can be achieved with a vibrational motor. Vibrational feedback may be divided into two sub groups which are proportional [10–12] and binary [13, 14] feedback systems. In a proportional feedback system, feedback varies in proportion to the change in input. On the other hand, a binary feedback system does not depend on proportional change in input. If input exceeds a threshold value, binary feedback is given by the system. Skin stretch is another popular haptic feedback method [15–18]. Its working principle is based on strain on the skin of various body parts in order to give feedback. Mechanoreceptor response is very high when the skin is subjected to strain [19, 20]. Moreover, it was shown that the sensitivity of human skin in response to tangential force at various body parts is higher than the response given to applied normal forces [9]. Lastly, ETAs can be classified under two general groups, wearable devices and smart white canes that are given in detail in the following chapters.

1.3.1. Navigation Systems for Visually Impaired Persons based on Smart White Canes

Kumar et al. [21] presented an ultrasonic sensor based white cane for visually impaired navigation. In this study, ultrasonic sensors were attached to a custom design sensor platform to detect aerial and ground obstacles. Sensor responses were processed in a micro-controller and transmitted to user through a wearable audio speaker in the form of a vest.

Another ultrasonic sensor based study is conducted by Saaid et al. [22]. Approximate distance between an obstacle and a user was calculated with time of flight of ultrasonic waves and speed of sound. Similarly, the calculated distance is transmitted to the user with the help of an audio signal. For instance, frequent beep sounds mean that the obstacle was close to the user.

Vibrational feedback is one of the most popular methods in smart white cane studies. In the study of Gallo et al. [10], they developed a sensory instrumented handle which can be directly integrated into a classical white cane. This handle includes long and short range distance sensors for both surface and aerial obstacle detection. In the designed handle, the positions of three vibrating motors were located along the index finger and palm. These motors were activated in different spatiotemporal pattern for different obstacle detection cases. Kuchenbecker et al. [23] also suggested an attachment device for traditional white canes. The Haptic Alerts for Low-hanging Obstacles (HALO) system was designed as portable and affordable. It includes ultrasonic range sensor for obstacle detection and distance measurement. Eccentric mass motors created vibrational feedback for avoidance of low hanging obstacles.



Figure 1.1. A traditional white cane fitted with the smart system [23].

Agrawal and Gupta [24] worked on another smart white cane with vibrational feedback. Similarly, they used an ultrasonic sensor for obstacle detection, and a vibrator for feedback. However, this device also includes a GPS-GSM module to get real-time location of the user, and a panic button to inform users relatives in case of any emergency. Another feature that distinguishes this study from previously mentioned studies is that it included a water sensor, and gave the user a slippery floor warning to prevent possible accidents.

Another study is conducted by Meshram et al. [25]. NavCane is the device that can help people to find obstacle free paths for both indoor and outdoor environment. NavCane uses ultrasonic sensors to detect obstacles, and a water sensor to detect wet surface. These features are similar to the one of Agraval and Gupta [24]. Unlike the existing smart cane studies, the NavCane uses an RFID sensor to recognize objects with RFID tag in known indoor surroundings. All the environmental information are transmitted to user with the help of audio and vibrational feedback.

Takizawa et. al. [26] implemented a new concept for smart cane. Environmental recognition was provided by a Microsoft Kinect sensor. This device included an RGB camera, an infrared sensor and a three axes accelerometer. Color images and depth data were obtained by the RGB camera and the infrared sensor, respectively. In this study, smart cane recognizes the obstacles from depth data, and provides feedback via the tactile device.

In the study of Mancini et. al. [27], a modular sensor box is used for environmental recognition and path planning. This box includes an inertial measurement unit, ultrasonic sensor, short range LIDAR, and mid range automotive radar. All these sensor measurements are processed and fused in robot operating system (ROS).

Another study was conducted by Vaibhav et. al. [11] in which an ultrasonic sensors were used for obstacle distance measurement. Distance information was transmitted to the user through vibratory patterns that vary incrementally depending on measured distance. The system was designed to be detachable and light weight. And this device has turned into a commercial product.

1.3.2. Wearable Navigation System

Kanwal et al. [28] worked on a wearable obstacle detection and path planner system. This system included Microsoft Kinect module which had RGB camera and infrared sensor together. Obstacles were determined from camera output and corner

detection algorithms. Depth information of obstacles were obtained from Kinect's infrared sensor. Combination of these two information gave a robust and safe path suggestions to user. The suggested path was described with help of audio feedback.

Another study which also included Kinect module was conducted by Bai et al. [29]. RGB-D camera and inertial measurement unit were attached to eyeglasses. A lightweight Convolutional Neural Network (CNN) model was trained for object recognition and this model provided the semantic information of environment such as locations and orientations of obstacles. This system also included a smartphone which was used to obtain current position of user via its GPS module and deploy trained CNN model for object detection and navigation. All the navigational feedback was given with earphones.



Figure 1.2. Prototype of CNN based wearable assistive device [29].

Alderen et al. [30], Lin et al. [31] and Vlamincx et al. [32] also studied RGB-D camera based wearable navigation devices. They both used color and depth information

of images to detect obstacles and to generate safe walking path. Also, these works provided semantic map of surroundings to user. This map was used to classify obstacles as walls, floor, steps, doors and other common objects.

Pardasani et al. [33] worked on smart glasses and shoes. Both devices worked together and provided a safe navigation solution for visually impaired. Smart glasses included Raspberry Pi and camera which was used for object detection. TensorFlow Object Detection API is a pre-trained object detection model and it was used in this project. This model only recognized objects but could not give any information about distance to user. At this point, the smart shoes came into play, it measured the distance of the object from the user with the help of infrared sensor on it and the whole smart system guided the user with voice commands.

Priya et al. [34] studied face recognition, object detection and distance measurement methods by using ultrasonic sensors and camera. They activated ultrasonic sensor for the measurement of distance between obstacles and user at the first step. After that object and person recognition were completed with the Raspberry Pi and camera. All outputs were transferred to user via audio feedback.

Kumar et al. [35] worked on a smart hat which includes USB camera and sonar sensor. Obstacles within 300 cm can be detected with proposed system. Camera frames were used to determine properties of obstacles in particular and human presence. The necessary directions were made by audio feedback with the help of headphones.



Figure 1.3. Smart helmet system that can detects obstacles and transmits them to user via headphone [36].

In the study of Schwarze et al. [36], they developed smart bicycle helmet which included a binocular camera, headphones and an inertial measurement unit (IMU). Binocular camera frames were used to detect and track static and moving objects and classify them into predefined groups. Unlike previously mentioned vision systems which can detect obstacles of certain categories like cars, people, tree or pets based on their appearance. This system defined obstacles as an assembly of spatially adjacent points, which cannot be a part of the scene at background geometry. Audio feedback was used to narrate safe navigation path after evaluation of spatially neighbored points.

Another navigational aid device with audio feedback was created by Kotyan et al. [37]. In this study, 90 different types of objects were detected and their distance to user was calculated with the help of two camera. In addition, this prototype used Google Directions API to find safest and shortest direction via smartphone.

The audio feedback method was used in the studies mentioned so far. However, in the study of Scheggi et al. [14], vibrotactile bracelets were used to give navigational information to user. Environmental perception was provided by camera glasses and remote operator proper navigational information to blind user via vibration motors.



Figure 1.4. Dual channel human machine interaction system prototype [38].

In the study of Zhang et al. [38], stereo camera provided environmental perception and dual channel human machine interaction system can give desired navigational micro-instruction via vibrational haptic gloves and macro-long-term planning and situational awareness via headphones continuously.

Kiuru et al. [39] studied on radar technology to create assistive navigation device for visually impaired. In this work, mini radar device sent radio signal to environment and tried to detect obstacles by evaluating the returning signals. Outputs of obstacle detection algorithm were conveyed via sound and vibrational feedback.

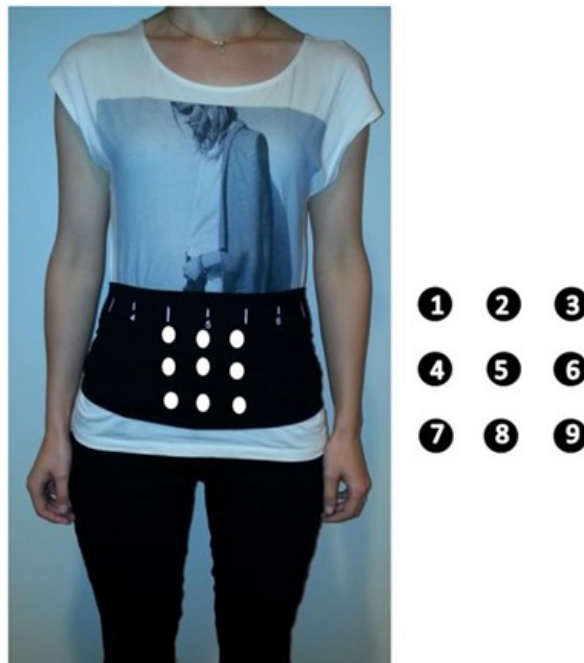


Figure 1.5. Tactile grid belt [40].

Erp et al. [40] focused on the required amount of tactile feedback mechanism of electronic travel aids and developed tactile feedback belt. In this study, vibrational feedback belt which included 3x3 tactor display was designed. The designed belt was shown in Figure 5. White dots demonstrated the location of tactors. Each tactor tried to express obstacle location such as top row tactors (1,2,3) described hanging obstacles, the middle row (4,5,6) described grounded obstacles and if there was no obstacles bottom row (7,8,9) tactors were activated. The position of obstacles were

also classified according to their direction, factors (1,4,7) represented obstacle from the right, the middle factors (2,5,8) showed obstacle in front and factors (3,6,9) expressed obstacles from the left.

In the study of Katzschmann et al. [41], there were two belts which included array of LIDARs and vibrotactile units. This device detected low and high hanging obstacles and also physical boundaries of surroundings with the help of sensor belt. TOF sensors were attached to sensor belt and sent infrared light pulses to measure distances between the user and obstacles. This measurement information was transferred to user via haptic belt which included vibrational motors.



Figure 1.6. Sensor belt is located at bottom and haptic belt is located at top [41].

Another tactile belt study was conducted by Palleja et al. [42]. In this study, LIDAR and tri-axial accelerometer were attached to the user's forearm and act like a virtual white cane. Information about surrounding were expressed via tactile stimuli on the skin by using vibrational elements which were located at haptic belt.

Vibro tactile belts are common solution to visually impaired navigation. In the study of Cosgun et al. [12], different vibrational patterns were tried to get the most intuitive way to navigate users. There were two main classes for vibrational patterns which were directional and rotational. Directional patterns excited a navigation towards a direction. Whereas, rotational patterns excited a rotation around self and try to change orientation of the human body.

Valezquez et. al. [13] worked on navigational device that consisted of a set of vibrational motors embedded in a foam shoe-insole. Perceptual experiments were conducted and final design included 4 vibrating motors to navigate user forward, backward, right and left.

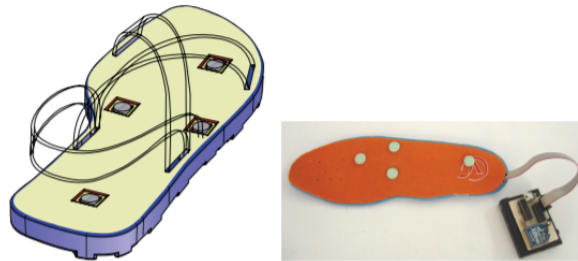


Figure 1.7. Vibrotactile foam shoe insole design [13].

Another wearable solution was conducted by Kon et. al. [43]. In this study, three different devices which focused on hanger reflex at head, waist, and ankle were developed. Hanger reflex can be defined as an unintentional position change of the human body with the desired forces which were applied to the different parts of the body. Head, waist, and ankle type of hanger reflex devices were used to navigate blindfolded person in the study of Kon et. al. [43].

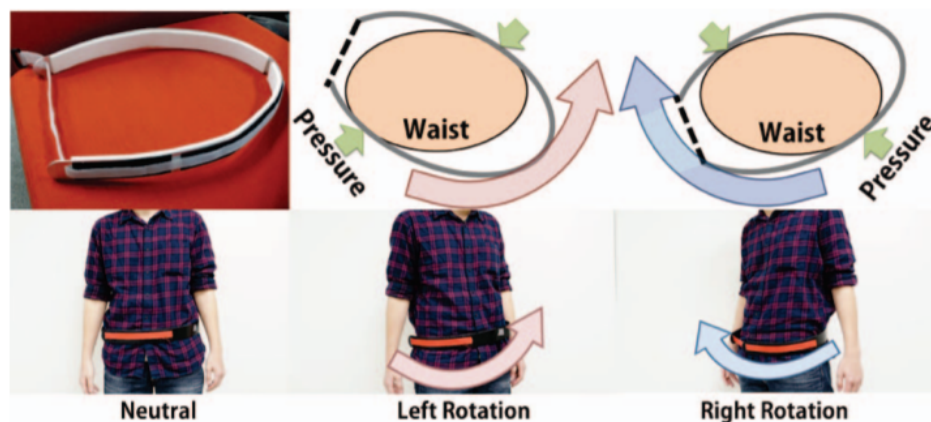


Figure 1.8. Waist type hanger reflex device and working principle [43].

1.3.3. Navigation Systems for Visually Impaired Athletes

Before mentioned studies were mostly focused on safe path planning, obstacle avoidance and these assistive studies did not aim to make sport activities possible for visually impaired people. However, there were some works which had been developed in order to make doing sports easier for visually impaired.

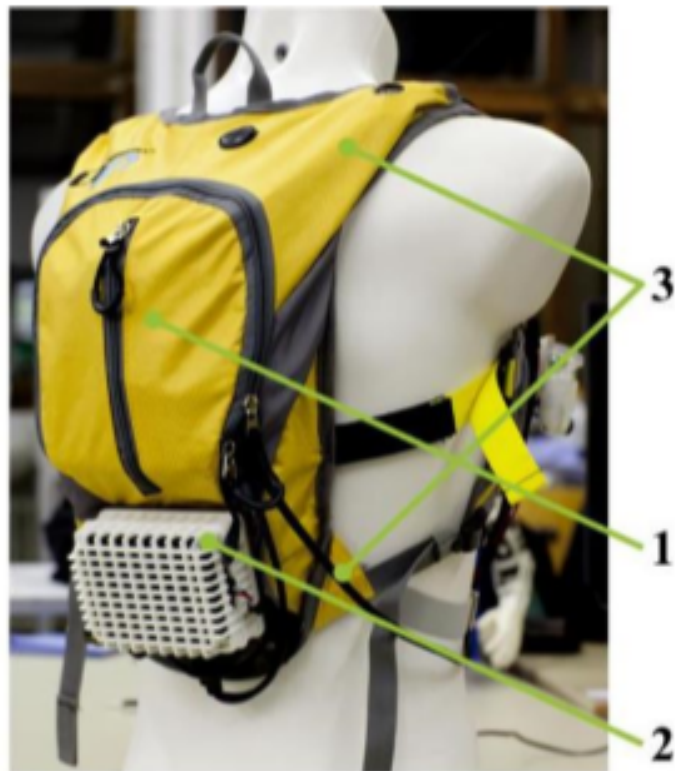


Figure 1.9. Backside of the prototypic structure of the integrated navigation device. Consisting of light backpack (1), processing unit (2) and integrated vibration motors in the straps (3) [6].

In the study of Ramer et al. [5], wearable jogging navigation system was developed. This system included course detection and collision avoidance algorithms for standard running track and also generated feedback in an intuitive manner with a vibrotactile belt. And in another study Ramer et al. [6] improved previous system and

worked on an adaptive lane detection method to use their device in general and less structured paths.

Skripko et al. [7] also focused on visually impaired's running activities. In this study, localization task in stadium or an analogical large space was provided with radio signal strength measurements. Positional information was transferred to user via voice command and vibration producing elements.



Figure 1.10. EyeVista track detection and warning [2].

Peiris et al. [2] studied on a light weight and low-cost wearable navigational assistive jacket which was called EyeVista. In this design, Raspberry Pi was used to process the real time image which was captured by Raspberry Pi camera to navigate the athletes with in a running track.

2. MATERIALS AND METHODS

2.1. System Overview

The proposed haptic guidance system consists of a Raspberry Pi, a Pi Camera (RGB), two servo motors, four pulleys and a battery (See Figure 2.1). All these pieces are attached on a fabric belt which can be adjusted with a buckle on the back of the waist. The system starts working by streaming of the Raspberry Pi camera to get environmental information. The camera streams are processed by the Raspberry Pi. Outputs of the environmental recognition and lane detection algorithms (See Sec. 2.2) are transmitted to the left and right pulleys via motion of the servo motors. A plastic material which can grip human skin is attached to these pulleys. In this way, algorithm outputs are transferred to the user by the skin stretch method.

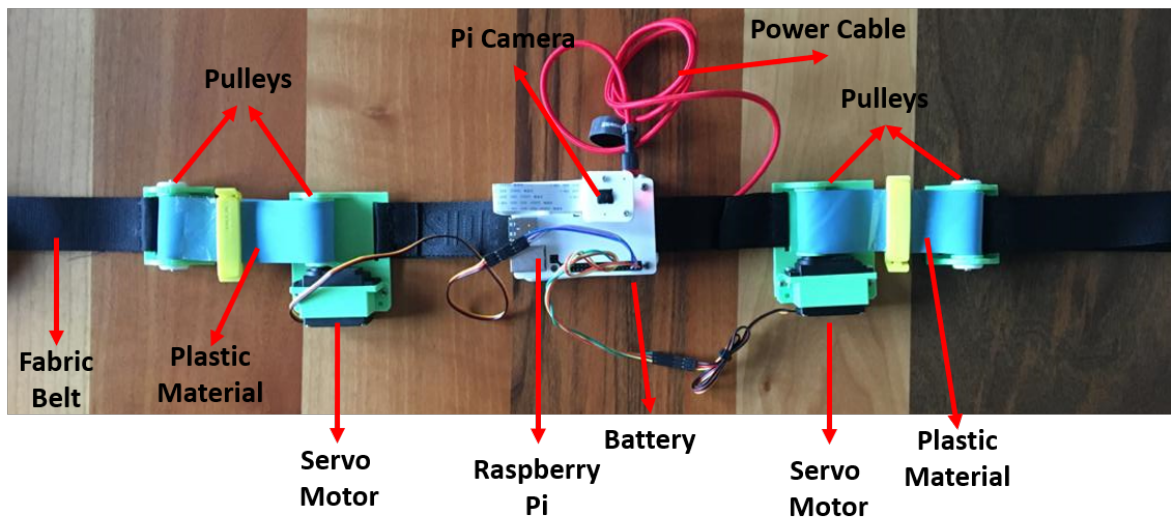


Figure 2.1. Prototype of the haptic guidance system.

2.2. Lane Detection Algorithm

2.2.1. General Detection Pipeline

Identifying lanes on a running track is the first part of this study. Haptic feedback will be given according to turning angle of the lanes which can be found by processing the frame. In order to create lane detection algorithm, Python language is used. Python can serve powerful libraries such as OpenCV for image processing and NumPy for scientific computing.

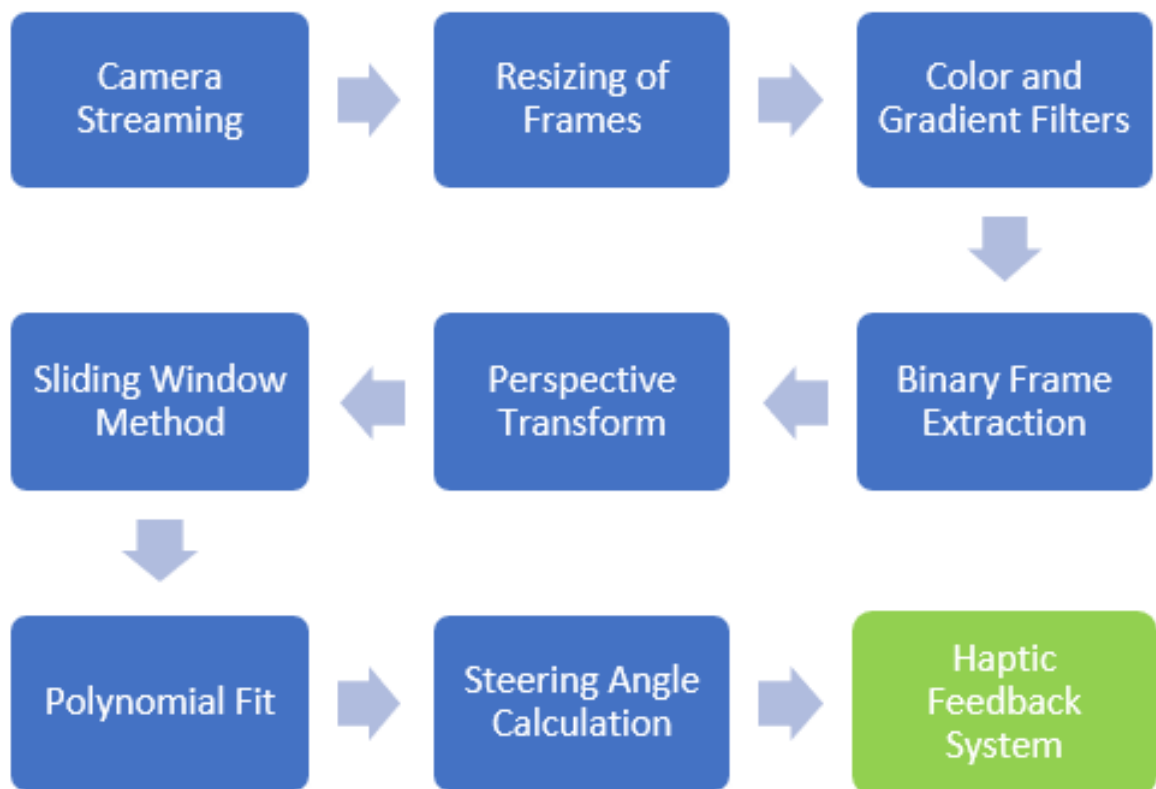


Figure 2.2. Lane detection pipeline.

As can be seen in Figure 2.2, frames obtained from the camera are the input for the lane detection algorithm. This algorithm includes color and gradient filters converting each frame into a binary matrix. Then, perspective transform is used to map a normal frame to a bird's eye view version to obtain lanes more clearly. After this,

the distribution of ones and zeros in the binary matrix is analyzed, and the starting points of the lanes are determined. Finally, the sliding window approach is applied to detect non-zero pixels of the binary frame, and a second-degree polynomial is fitted to these non-zero pixels. Coefficients of the second-degree polynomials are used to calculate steering angle of the servo motor which is an input of the haptic feedback system.

2.2.2. Image Spaces and Color Filters

Color segmentation or color filtering is widely used in machine vision algorithms to detect objects, regions and lanes. The most common color space is RGB which is an additive color space comprised of three color shades (Red-Green-Blue). Each component of these shades can take a value between 0 and 255. For example, (0,0,0) tuple expresses black and (255,255,255) tuple expresses white color. Other colors can be represented as combination of these three channels. In addition to RGB, two other color spaces are used as well: HSV and HLS. These color spaces can separate the pixel intensity from the color information. Hue (H) expresses dominant wavelength, saturation (S) channel expresses shades of color, Value (V) and Lightness (L) channels describe intensity information of the image.

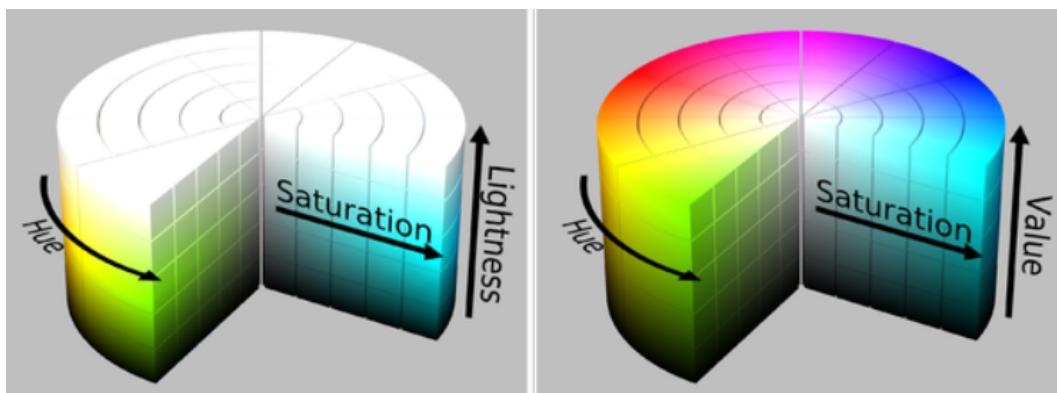


Figure 2.3. HLS and HSV color spaces representation.

In the image segmentation part, separating color information from intensity is quite critical for the robustness of the algorithm to lighting changes. These lighting

changes can be observed while running on the track. In order to get a robust algorithm, different color spaces and different color filters were tried. In Figure 2.4, all channels of an unfiltered frame are shown. Some of the channels can be very useful to filter lanes, while others contain extremely noisy and indistinctive results. All color channels (Red, Green, Blue, Green-Red, and Blue-Yellow) are very sensitive to lighting changes, and can not be an option for a robust color filtering. In addition to this, Hue channel does not contain any distinctive information about track lanes. After experimenting with many different frames, it was found that the lane lines in the Lightness and Saturation channels were more distinct. Therefore, Saturation and Lightness channels are the best options for required filtering.

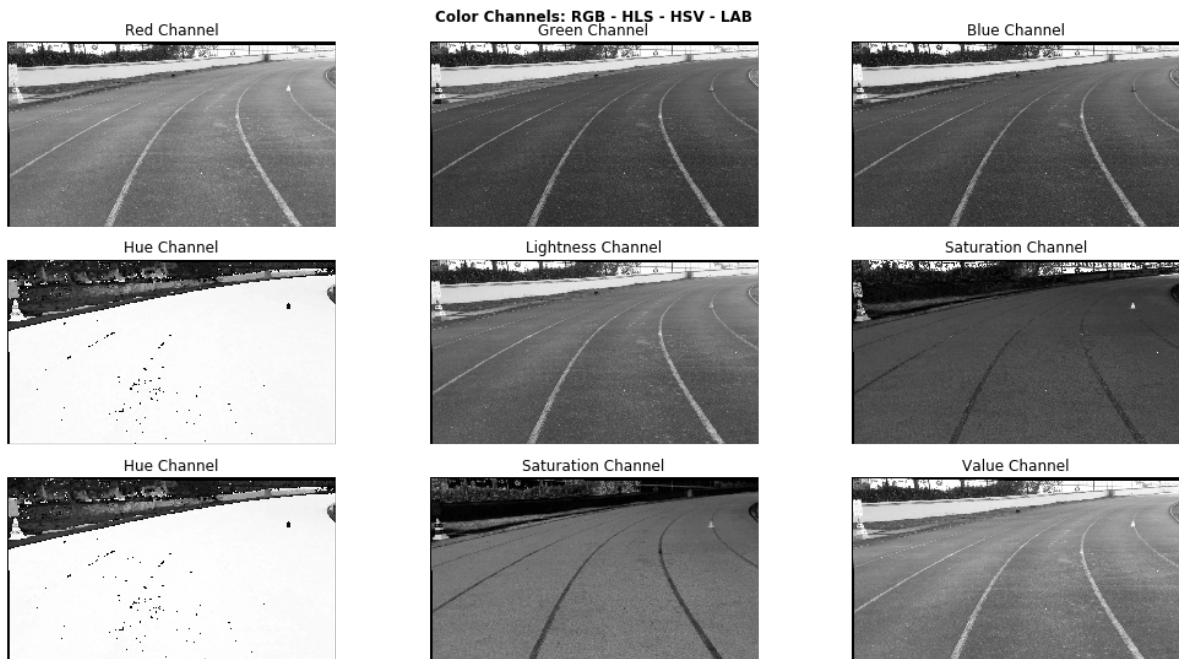


Figure 2.4. RGB-HLS-HSV view of specific frame.

HSV and HLS color spaces are used to filter each frame. First of all, each RGB frame should be transformed into HSV and HLS color spaces. In order to do these transformations, the built-in functions in OpenCV library `cv2.COLOR_RGB2HSV` and `cv2.COLOR_RGB2HLS` are used. In case of RGB to HSV transformation, V channel

is determined from maximum value among R, G, and B channels.

$$V = \max(R, G, B) \quad (2.1)$$

If V channel is not equal to zero, then S channel can be calculated by the following formula:

$$S = \begin{cases} \frac{V - \min(R, G, B)}{V}, & V \neq 0 \\ 0, & \text{otherwise} \end{cases} \quad (2.2)$$

Finally, H channel calculation depends on 3 different cases which are related to maximum value of R, G, and B channels.

$$H = \begin{cases} \frac{60(G-B)}{(V - \min(R, G, B))}, & V = R \\ 120 + \frac{60(B-R)}{(V - \min(R, G, B))}, & V = G \\ 240 + \frac{60(R-G)}{(V - \min(R, G, B))}, & V = B \end{cases} \quad (2.3)$$

In case of HLS transformation, calculation of H channel is the same as in Equation 2.3, but L and S channel values are derived using the following formulas:

$$\begin{aligned} V_{max} &= \max(R, G, B) \\ V_{min} &= \min(R, G, B) \end{aligned} \quad (2.4)$$

$$L = \frac{V_{max} + V_{min}}{2} \quad (2.5)$$

$$S = \begin{cases} \frac{V_{max} - V_{min}}{V_{max} - V_{min}}, & L < 0.5 \\ \frac{V_{max} - V_{min}}{2 - (V_{max} - V_{min})}, & L \geq 0.5 \end{cases} \quad (2.6)$$

In order to obtain a robust algorithm, different filters were tried. The main principle of image filtering is to determine upper and lower boundary conditions for each channel. Binary transformation of the frame is made according to these boundary limits. If a pixel value is within these limits, it is assigned as one. Otherwise, its value is changed into zero.

After a trial and error process, upper and lower boundary values for the S channel filter are determined as 50 and 0 respectively. The L channel filter is also applied to the frame, and the upper and lower values of this filter are selected as 80 and 0. These filters were tested on many different frames with determined thresholds. However, the combination of these filters gave a more robust results (See Figure 2.5) than applying them individually.

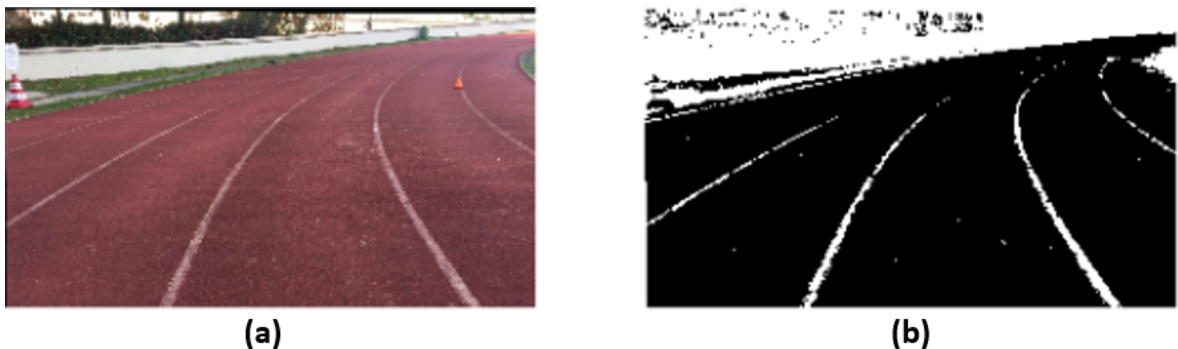


Figure 2.5. a)Unfiltered frame, b)Filtered with combined (S and L) channels.

2.2.3. Gradient Filters

Another filtering technique is related to pixels gradient which is a directional change in intensity of a frame. In order to get image gradient information, differential operators which are also known as masks or kernels are used. These kernels returns derivatives of each pixels in the specified direction. One of the methods to calculate derivatives is using the Sobel operator. It computes an approximation of the gradient of an image.

Gradient approximation in x direction is calculated with S_x kernels in Equation 2.7. Vertical gradient change can be calculated using S_y kernels in Equation 2.8. These kernels can be in different sizes such as 3x3, 5x5, 7x7 and so on.

$$S_x = \begin{bmatrix} -1 & 0 & 1 \\ -2 & 0 & 2 \\ -1 & 0 & 1 \end{bmatrix} \quad (2.7)$$

$$S_y = \begin{bmatrix} -1 & -2 & -1 \\ 0 & 0 & 0 \\ 1 & 2 & 1 \end{bmatrix} \quad (2.8)$$

After convolution operation is conducted with these directional kernels, gradient information matrix for each frame is created. Then, different threshold values are tried to get effective filtering. The results of horizontal and vertical gradient filters for all tried sizes of kernels and threshold values are shown in Figure 2.6 and Figure 2.7 respectively.

Other than directional gradient filtering, Sobel operators can be used to find gradient magnitude and direction. The square root of the sum of squares of vertical and horizontal gradients gives the gradient magnitude. Direction of gradient can be calculated with Equation 2.10. These features can also be used to filter image to get robust lane detection algorithm. Kernel sizes and threshold experiments were also done with these features but there is no significant improvement for algorithm robustness and also these features calculations need more calculation power.

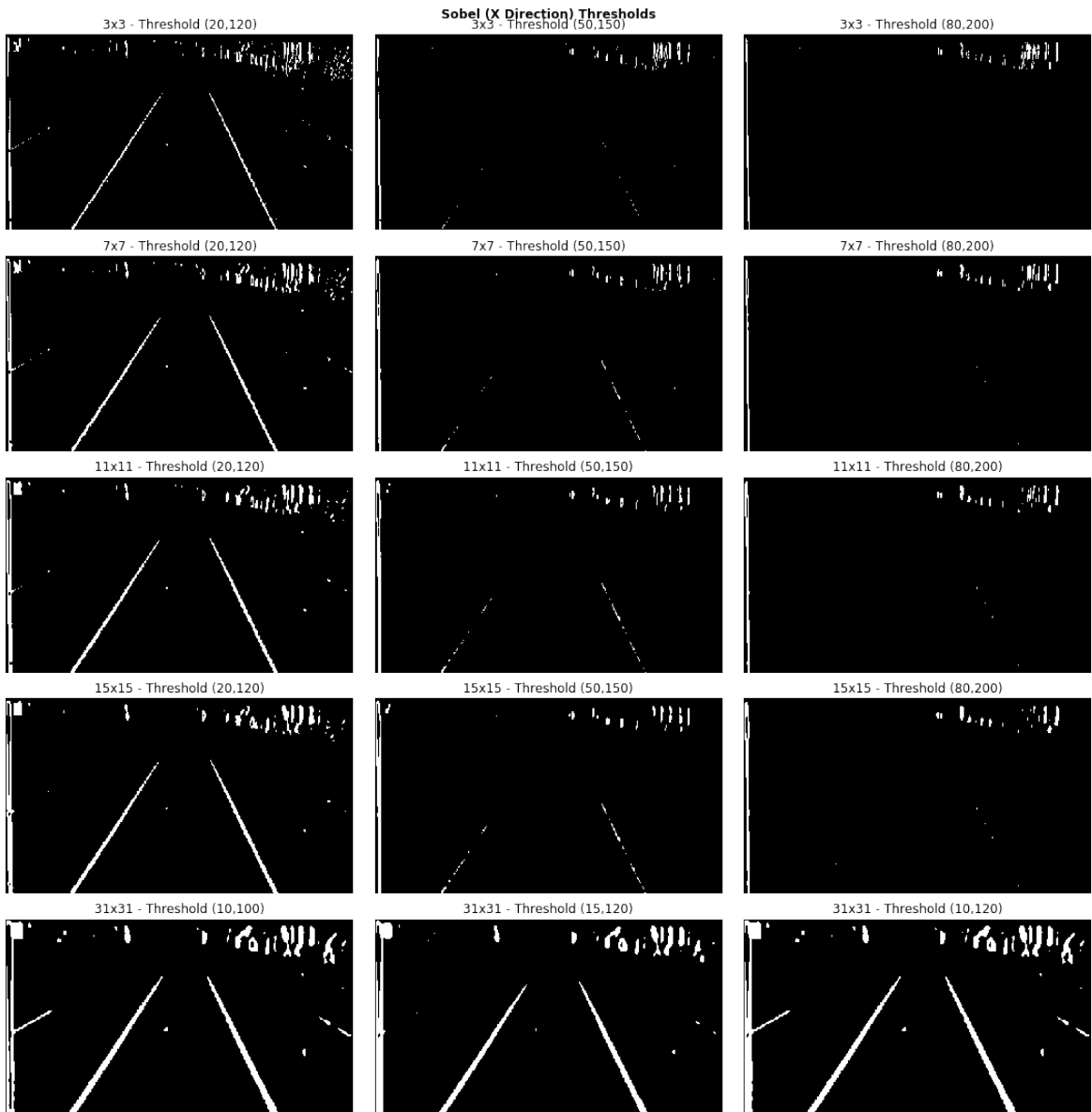


Figure 2.6. Horizontal gradient filter results.

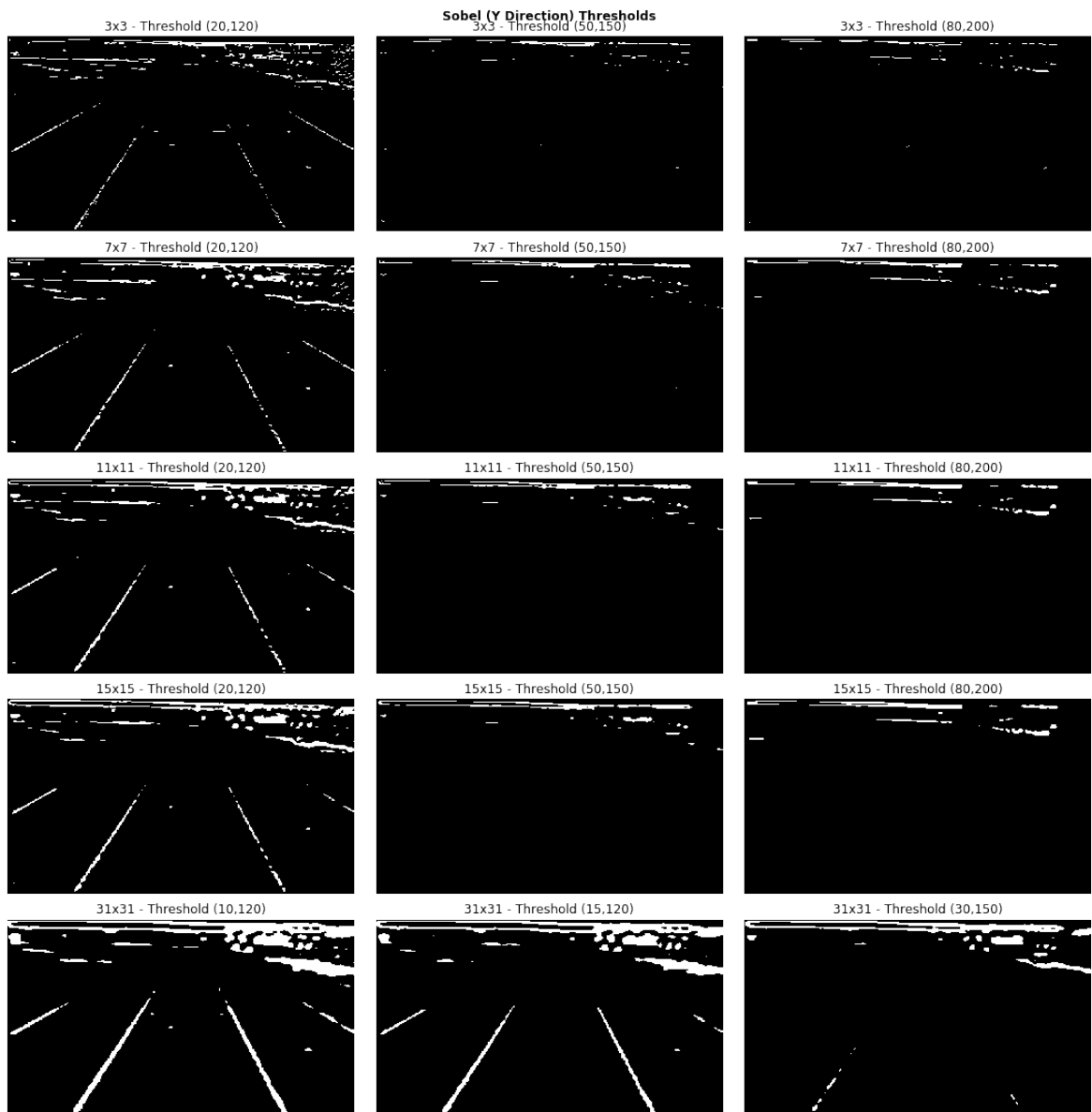


Figure 2.7. Vertical gradient filter results.

$$S_{xy} = \sqrt{S_x^2 + S_y^2} \quad (2.9)$$

$$\theta = \arctan\left(\frac{S_x}{S_y}\right) \quad (2.10)$$

Combination of gradient filters and color filters makes algorithm more robust. Therefore, horizontal gradient filter, hue and lightness channel filters are used together to detect lane lines.

2.2.4. Perspective Transform

Track lanes are easily distinguished by humans, but the task of determining the exact direction of the lanes is hard using RGB camera frames. Objects further away from the camera appear smaller in the frame, and the track lanes tend to overlap as they are further from the runner, which is not a true reflection of the real case. This problem is called perspective distortion. One of the solution to this problem is transforming the images into bird's eye perspective, given as

$$M = \begin{bmatrix} -128 & -120 & 32400 \\ 0 & -192 & 17280 \\ 0 & -0.47 & 1 \end{bmatrix}. \quad (2.11)$$

The OpenCV library provides the functions *getPerspectiveTransform* and *warpPerspective* to conduct this transformation. The first objective is to determine source and destination points from the original frame. Then, *getPerspectiveTransform* function calculates the transformation matrix given in Equation 2.11 from these points. Finally, the bird's eye view version of the original frame is created with *warpPerspective* function and *M* matrix.

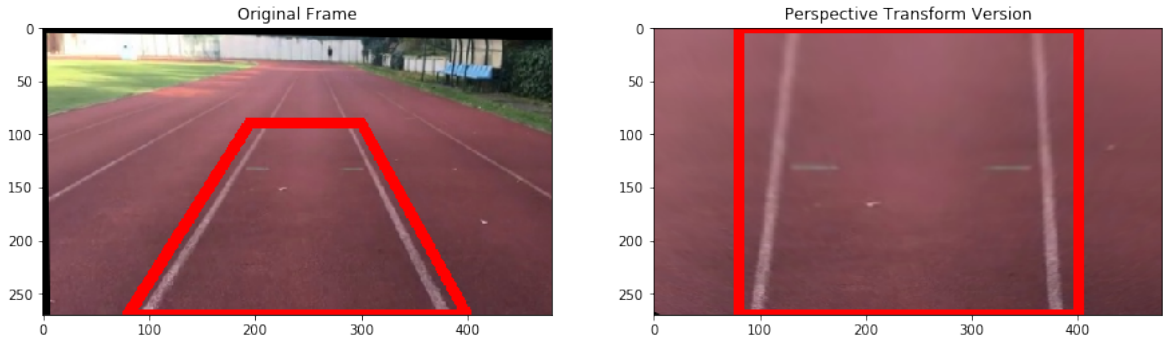


Figure 2.8. Original frame and perspective transform result.

2.2.5. Sliding Window Algorithm and Polynomial Fits

The original frame is converted into a binary frame with the perspective transform, color and gradient filters. The binary frame consists of ones and zeros and pixels that have a value of one are defined as hot pixels. The next issue is to mask left and right lanes hot pixels. A sliding window algorithm is used to decide which pixels are part of these lanes. First of all, initial position of the lanes are determined with a histogram of the bottom half image. The sliding window algorithm for both left and right lanes starts from the peaks of this histogram. The image is divided into horizontal strips, and sliding windows try to detect left and right peaks for each strip. The algorithm checks hot pixels ratio inside the window, and if the ratio is less than 0.85, the window starts to slide left or right to obtain this ratio. The pixels inside the window are labeled pixel of interest, and these pixels compose left and right lanes. Mean x and y values of pixels in each sliding window are passed through the OpenCV polyfit function, and the second degree polynomial coefficients (A, B and C in Equation 2.12) are calculated, as

$$\begin{aligned} x_{right} &= A_r y^2 + B_r y + C_r \\ x_{left} &= A_l y^2 + B_l y + C_l. \end{aligned} \tag{2.12}$$

2.2.6. Curvature Calculation and Steering

After finding polynomial fits of lanes, curvature calculations are needed. The radius of curvature of the finding lanes at a particular point can be defined as the radius of approximating circle which shares the same tangent and curvature with detected lanes [44]. Radius of curvature is an important parameter and it will be an indicative to the steering angle of the runner. Previously, left and right lanes boundaries are approximated as a second order polynomial curves in Equation 2.12. Radius of curvature of an arbitrary point of these lanes can be calculated with the following formula:

$$R_{curve} = \frac{[1 + (\frac{dx}{dy})^2]^{\frac{3}{2}}}{|\frac{d^2x}{dy^2}|}. \quad (2.13)$$

If the derivatives of the second order polynomial are calculated, radius of curvatures of each lane can be represented with

$$R_{curve} = \frac{[1 + (2Ay + B)^2]^{\frac{3}{2}}}{|2A|}. \quad (2.14)$$

2.2.6.1. Pixel to meter transformation. Another consideration before the radius of curvature calculation is images are in pixels whereas the real world is in meters. Therefore, pixel to meter transformation is needed. This transformation is also crucial to detect exact location of the runner in the lane. Distance between lines are 320 pixels in image and the real world case is measured as 1.22 meters. Distance between exact position of the runner and a reference point in y direction is measured as 270 pixels in the image space, and 3 meters in the real world. Transformation coefficients are calculated for both x and y axes, as

$$\begin{aligned} X_{c_{perpx}} &= 1.22/320, \\ Y_{c_{perpx}} &= 3/270. \end{aligned} \quad (2.15)$$

In actual usage of the prototype, the camera is expected to be mounted exactly at the centre of the runner's waist. This means that the center of each frame should match with the lane center. In order to calculate the offset from the centre, x axis values which are right and left lines crossed near the runner should be determined. The lane centre is the mean of right and left lines x values in Equation 2.16. Difference between the lane center and the image center can express runner's offset to the middle of the lane. If this pixel difference is multiplied with Xc_perpx (transformation coefficient), real world offset can be calculated, as

$$x_{lane-centre} = x_{right} - x_{left}. \quad (2.16)$$

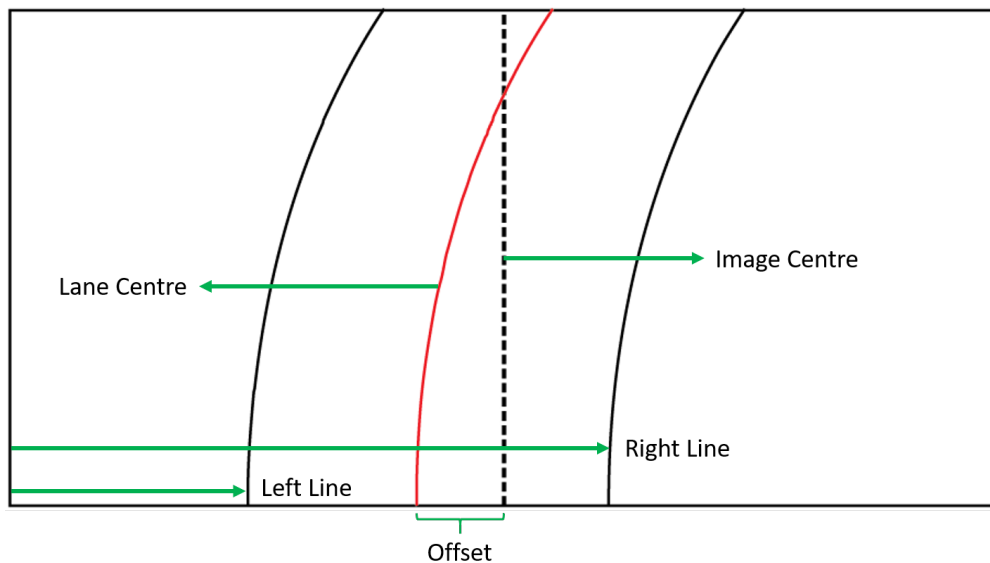


Figure 2.9. Lane centre offset illustration.

The real world offset and curvature values are used for the steering calculation and direction determination. The large curvature values for left and right lines indicate that the running lane does not contain any bend and continues straight. The offset value for forward reference point are used to determine lane turning direction. Steering

angle calculation is conducted with a reference point offset value and the actual distance between the runner and the reference point,

$$\theta_s = \arctan\left(\frac{ref_{offset}}{ref_{distance}}\right). \quad (2.17)$$

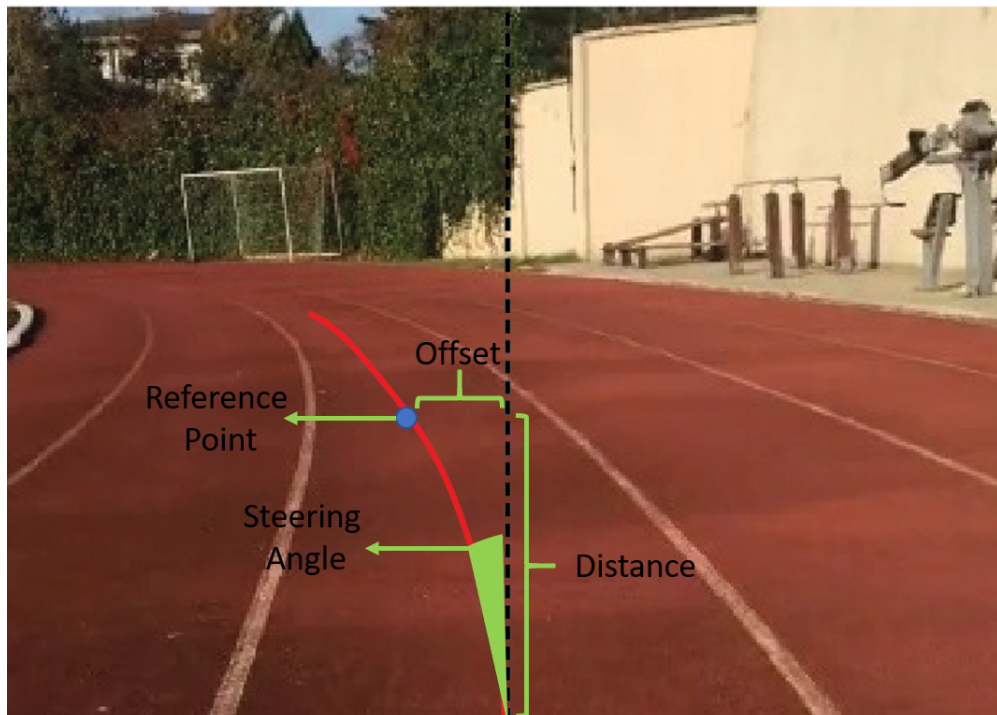


Figure 2.10. Steering angle calculation parameters of the reference point.

2.3. Servo Control

After calculating the steering angle, this information need to be transferred to the user, namely a visually impaired runner. A servo motor and a plastic material which can grip human skin are used to transmit the desired angle. Servo motors can provide precise angle control and this feature makes them a more proper choice for this case. Inside a servo motor, there are four main components, a small DC motor, a potentiometer, a gearbox and a control circuit. When the motor rotates, resistance of the potentiometer changes, and the control circuit can regulate movement direction and amount.

One of the servo motor working principle is cutting the power supply to the motor, if the servo is at the desired position. Also, the motor's speed is proportional to the difference between the desired position and current position. Slow movement speed of servo indicates that actual position is close to the desired position. Moreover, the desired position of the servo motor can be set with electrical pulses with variable width or pulse width modulation (PWM).

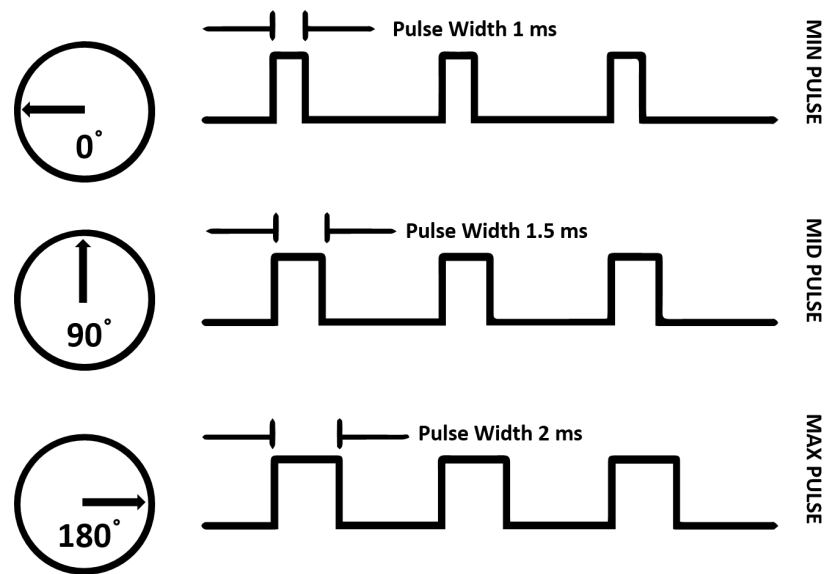


Figure 2.11. Servo position for different signal width.

Most of the servos can usually only rotate 90 degrees in both directions. Position of the shaft is determined with a PWM pulse. Duration of the signal is a control method for position. A usual servo motor expects to see the signal in every 20 milliseconds (ms). If the desired position is set to 90 degrees, the PWM signal should be sent for 1.5 ms. Shorter signal moves servo in the counter clockwise direction toward the 0 degree position and longer signal drive servo in clockwise direction to 180 degree position.

In this study, HS-311 servo motors are used, and the calculated steering angle is transmitted to servo motors via GPIO pins of Raspberry Pi. Duty cycle of the motors is regulated with respect to the steering signal.

2.4. Haptic Feedback System Design and Working Principle

Skin stretch feedback is used for guidance of the visually impaired runners. This haptic feedback system is designed as a belt which includes two servo motors (Hitec HS-311), a microcontroller (Raspberry Pi 4 Model B), an RGB camera (OV5647), a battery, a belt and a pulley system (See Figure 2.12).

The camera, control and power units are attached to the front of the belt. On the other hand, the servo motors and pulley system are located at both left and right side of the belt. In order to get better skin grip, a plastic material is used and attached to the pulley system. All the lane detection and servo steering algorithm runs on Raspberry Pi. Algorithm performance varies between 7 and 10 frame per second, which is enough for runner navigation. Main idea of steering calculation is keeping the runner in the middle of the lane. Desired steering angle calculated with the detected lanes polynomials.

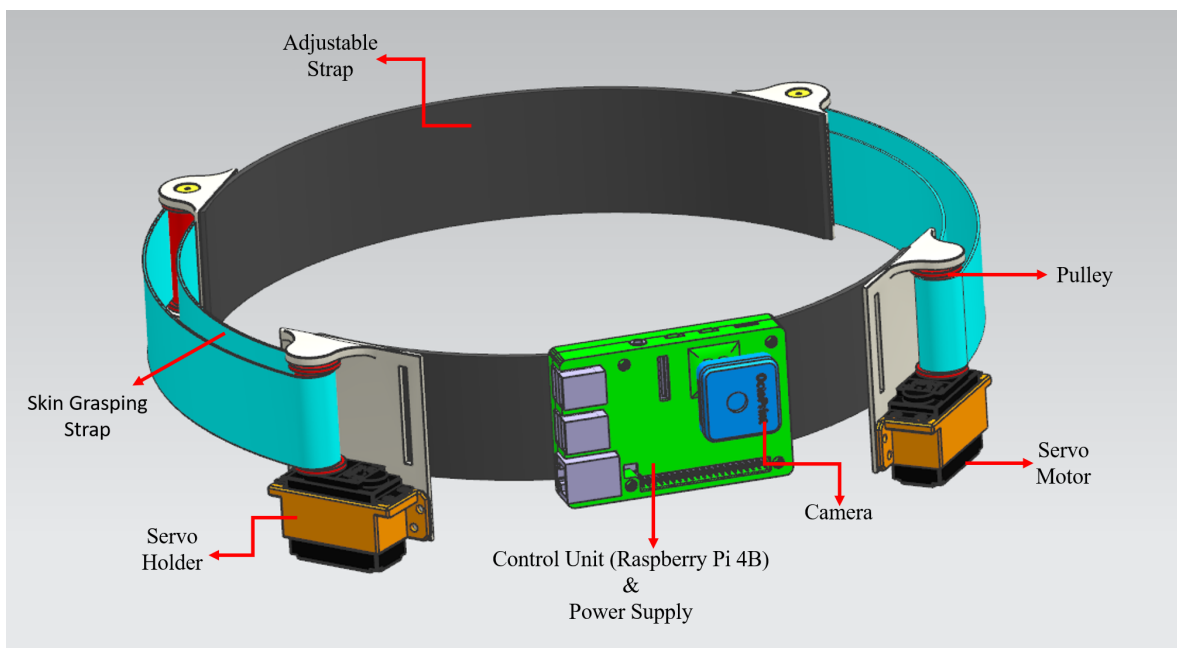


Figure 2.12. CAD model of prototype.

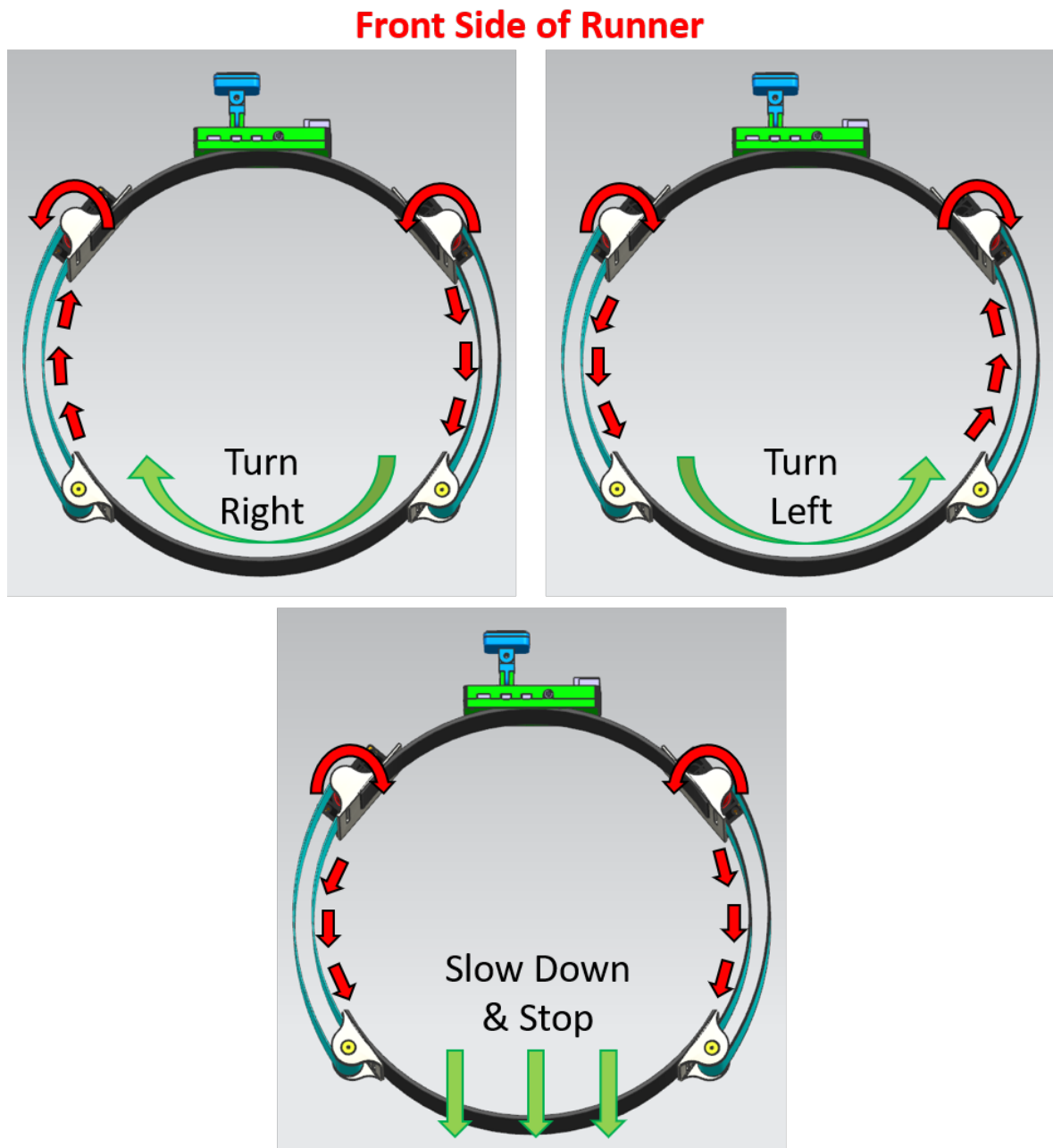


Figure 2.13. Desired feedbacks of prototype.

Movements of the designed system is given in Figure 2.13. If the user needs to turn right, both servos rotate counter clockwise direction, right part of the waist skin is stretched backward, and left part of the waist skin stretched forward. If the running lane curves left, the user should be directed to left. Therefore, both servos rotate clockwise direction and right part of waist skin is pulled forward while the left part is pulled backward. If the lane detection algorithm cannot find any left or right lines to track due to an obstacle or a deformed lane lines. The left servo rotates clockwise, the right servo rotates counter clockwise, and both sides of the waist skin are stretched backward to avoid any dangerous situation such as obstacle collision and going off the lane. Desired rotation angle of servo motor is derived from steering angle calculation step of lane detection algorithm.

2.5. Skin Stretch Physical Modelling and Calculations

Since it has been decided to use the skin stretch method to create a desired feedback, the physical properties of the skin have to be determined. The human skin can be deformed when the sufficient force is applied to the skin. Needed torque value from actuators has to be calculated with respect to the skin response. Skin stretch topic is widely investigated area, there are several tests have been conducted such as tensile, indentation, suction and torsion to reveal skin mechanical behavior. In the study conducted by Bark et al. [45], the experiments show that the human skin acts non-linearly for rotational and linear skin stretch tests. Therefore, the human skin stiffness is not constant, and can vary with respect to amount of stretches. In this study, relationship between the amount of skin stretch and the required force is modeled as a second order polynomial which is calculated from the Bark et al.'s experiment results [45]. Skin stiffness is derived from this polynomial and its formula is shown in Equation 2.18. In this study, the human skin is modeled as a spring, and stiffness of the spring can vary according to this equation. The desired torque calculation have been conducted with a string-skin analogy, given as

$$k_s = 0,007x + \frac{0,0754}{x} + 0,0194. \quad (2.18)$$

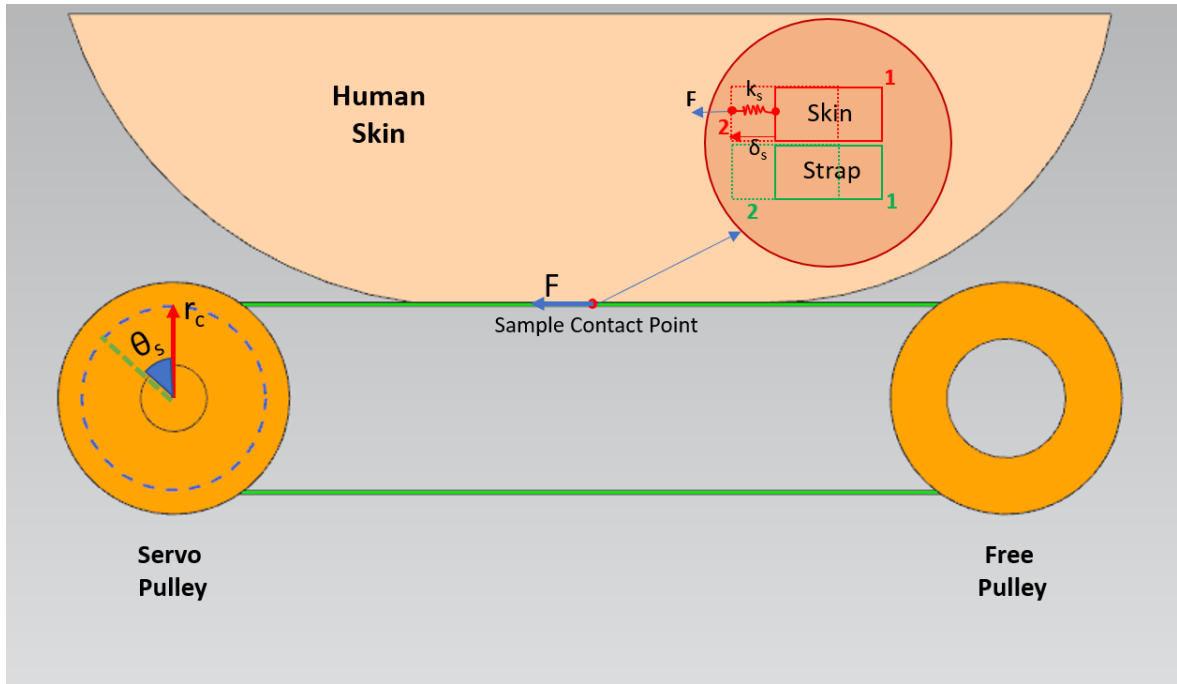


Figure 2.14. Illustration of skin-string analogy

In Figure 2.14, a string-skin assumption is visualized, and the required force is calculated with Equation 2.23. Servo motor selection is conducted with this force estimation. The desired force is dependent on the amount of skin stretch (δ_s). This value is directly related to the steering angle which is transmitted by the servo motors. In the figure, sample contact point position-1 is changed to position-2 with servo motor motion and skin is stretched with the force which is conducted with strap. The amount of movement is related to the steering angle, and pulley radius equal to 7.75 mm. This movement variable is also equal to the x value which is used in skin stiffness formula. Therefore, the desired force from the servo motor increases with respect to the amount of movement of skin. The relationships are given as

$$x_s = \left(\frac{\theta_s}{360}\right)(2\pi r_c), \quad (2.19)$$

$$r_c = 7.75 \text{ mm}, \quad (2.20)$$

$$\delta_s = x_s, \quad (2.21)$$

$$F_r = k_s \delta_s, \quad (2.22)$$

$$F_r = 0,000128\theta_s^2 + 0,002624\theta_s + 0,0754. \quad (2.23)$$

The required force with respect to the steering angle is plotted in Figure 2.15. Servo motor motion is limited to 90 degree for both clockwise and counter-clockwise directions. Therefore, the maximum required force to stretch the skin should be applied at 90 degree position. Having this level of movement ability is seen as sufficient to navigate visually impaired runners. The servo motors was selected by considering the maximum force value which was 1.35 N. Hitec HS-311 servo has 3 kg.cm maximum torque value according to its spec sheet which is shared at Appendix-A. This means that the motor and pulley combination can give 22 Newton at maximum torque. All these observations and calculations made this prototype capable of stretching the skin for the desired amount.

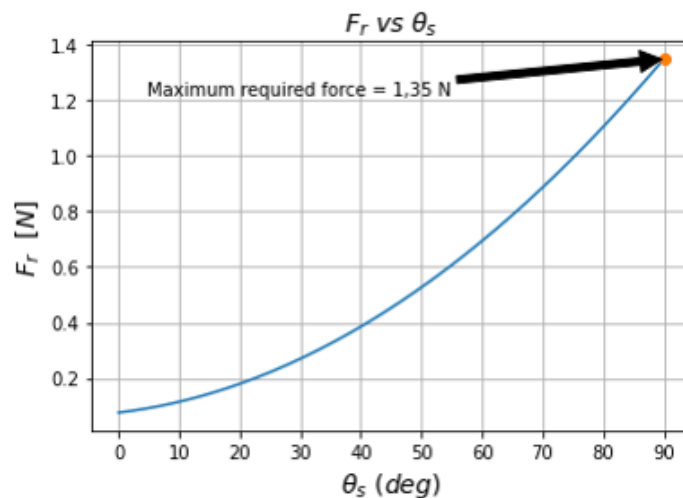


Figure 2.15. Required force and steering angle relation.

3. EXPERIMENTAL METHODS

The performance of the lane detection algorithm and haptic feedback system was evaluated with several tests. In this chapter, experiments are explained. Psychophysical experiments were approved by the Institutional Review Board of Bogazici University.

3.1. Lane Detection and Steering Calculation Tests

In order to test the lane detection and steering calculation algorithm, different video recordings were taken on the running track. In this test, complete prototype was used as video recording tool, feedback mechanism was disabled before the recordings. A total of twelve records were collected by the able-bodied user at two different speeds, three different lanes, clockwise and counter clockwise directions.

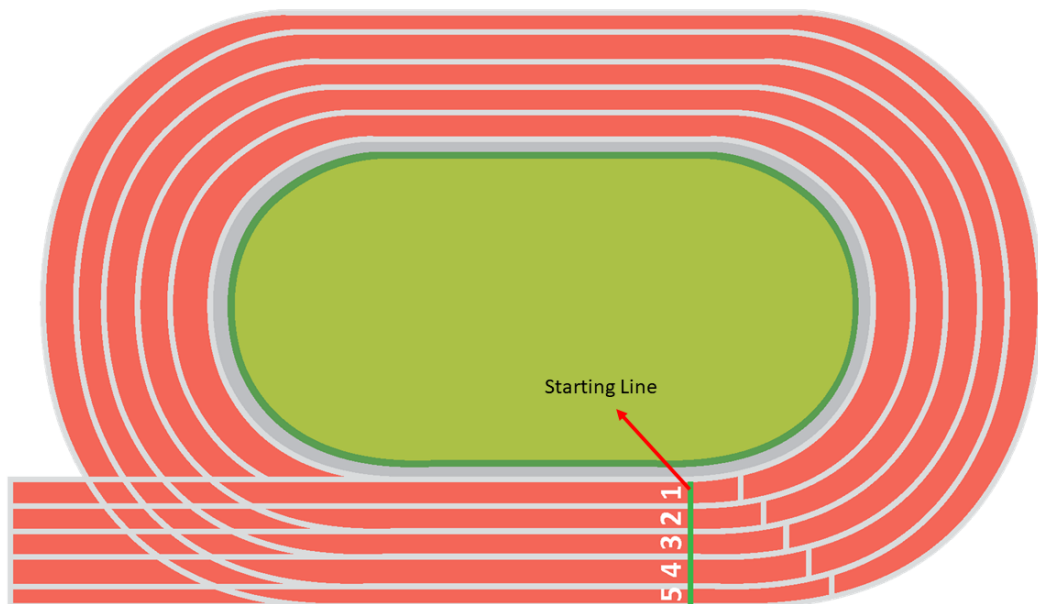


Figure 3.1. Running track illustration.

A running track is illustrated in Figure 3.1. Running lanes 1, 3 and 5 were used in clockwise and counter clockwise direction. One lap was approximately 400 meters and this distance was ran by user at an average speed of 5.5 and 6.6 kilometers per hour. After collecting running records, the desired steering angles of every seconds were calculated with the lane detection and steering angle calculation algorithms. These calculation results were compared with the steering angle assumptions of different region on the running track. It was assumed that the steering angle should be zero at straight part of the track, and should be the maximum steering angle of 45 degree in the turning region.

3.2. Skin Stretch Feedback Performance Tests

3.2.1. Static Tests

After the user adjusted the wearable prototype to his or her own body, he or she should be stayed at a stationary position. Meanwhile, random feedback was sent to the prototype, and the user should guess the direction and level of the feedback. After that, it was expected to fill the estimation chart in Figure 3.3. The desired feedback were divided into 15 degree intervals. In total 20 random feedbacks were sent and there was a certain time frame between each random feedback. The user should enter his estimation in this time interval. Before starting the test, a training session consisting of sample feedbacks were shown to the user and it was expected to get familiar to using the prototype.

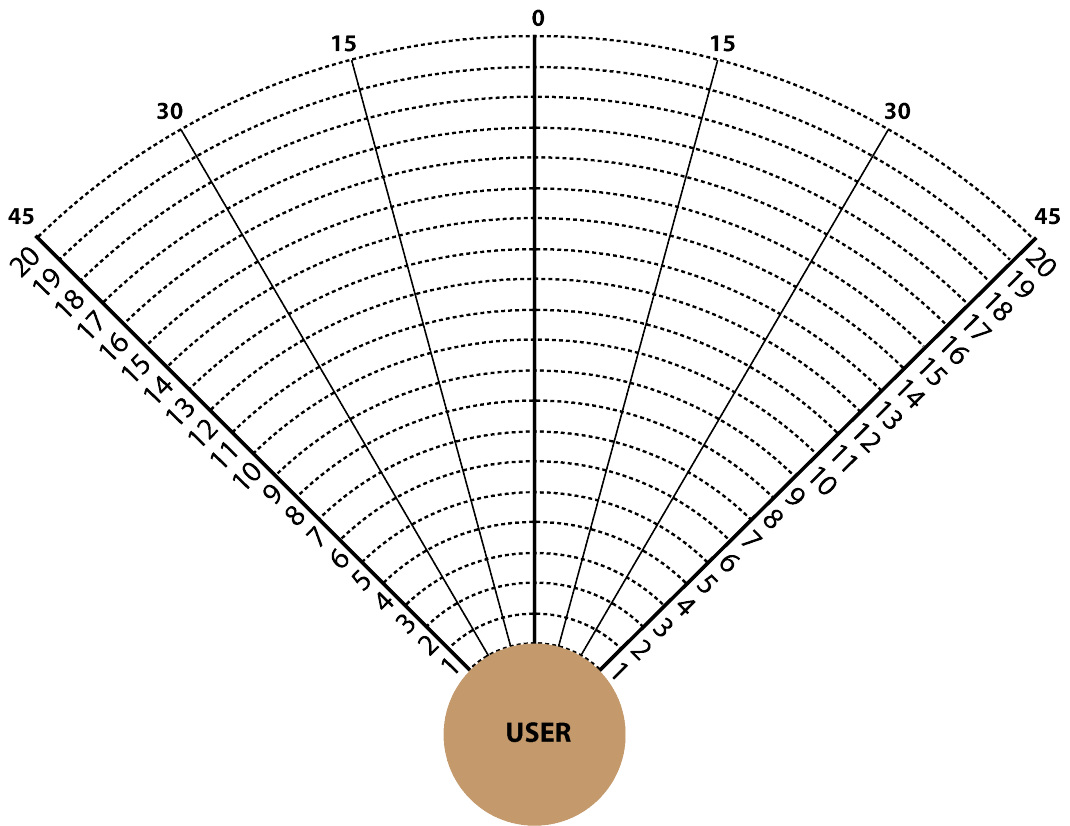


Figure 3.2. Static test estimation chart.

3.2.2. Pre-recorded Test

After the user adjusted the wearable prototype to his or her own body, the user should take the stationary position like in the static tests. Selected parts of the previously captured run records were sent to the lane detection and steering calculation algorithm, the desired feedback with respect to these records was given to user continuously. It was expected to convey direction and angle information of these continuous feedback from the user with the program interface which was specially designed for this experiment. This experiment was conducted with a combination of clockwise and counter clockwise direction running records. After that, the prototype feedback and the responses provided by the user through the interface were compared for every seconds.

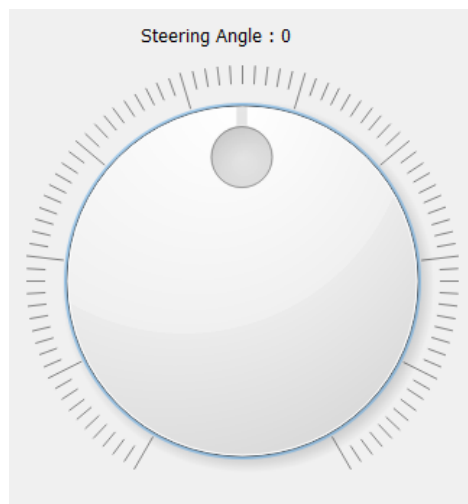


Figure 3.3. Pre-recorded test response collection interface.

3.2.3. Real-time Test

After the user adjusted the wearable prototype to his or her own body, the user should try to run blindfolded at the same lane of the athletic track. The experiment coordinator ran with the user for safety issues and evaluated the total performance of the system. In order to do that, the coordinator recorded failure situations such as time spent outside the desired lane and lane departures.

4. RESULTS and DISCUSSION

Results of the algorithm and haptic feedback experiments are given in this chapter. Overall performance of the wearable prototype is also discussed by considering all obtained results.

4.1. Algorithm Performance

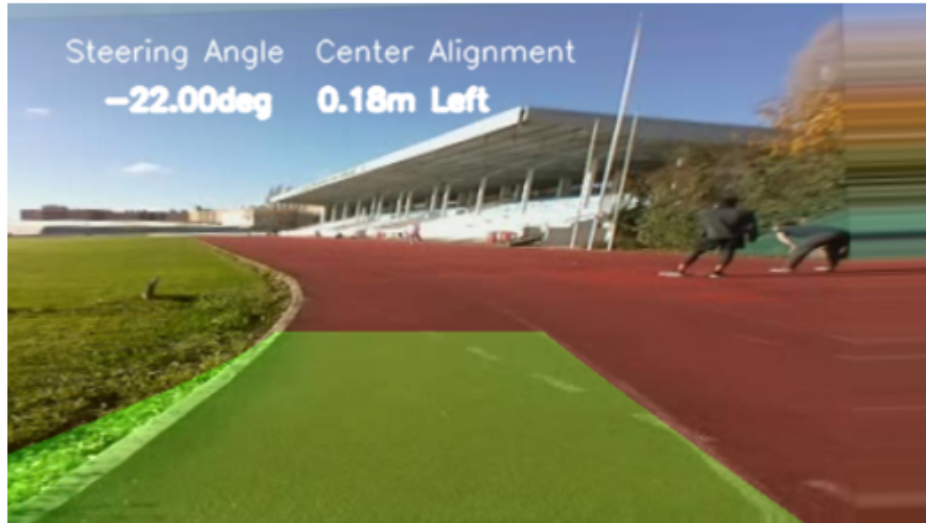
4.1.1. Lane Detection Performance

The lane detection algorithm took frames obtained by the camera, and detects track lanes and highlights them as in Figure 4.1. Overall performance of lane detection algorithm was calculated by comparing the time period of successfully detected lanes and total time of the video records. The mean success rate of the algorithm in all video recordings is 86.5 % .

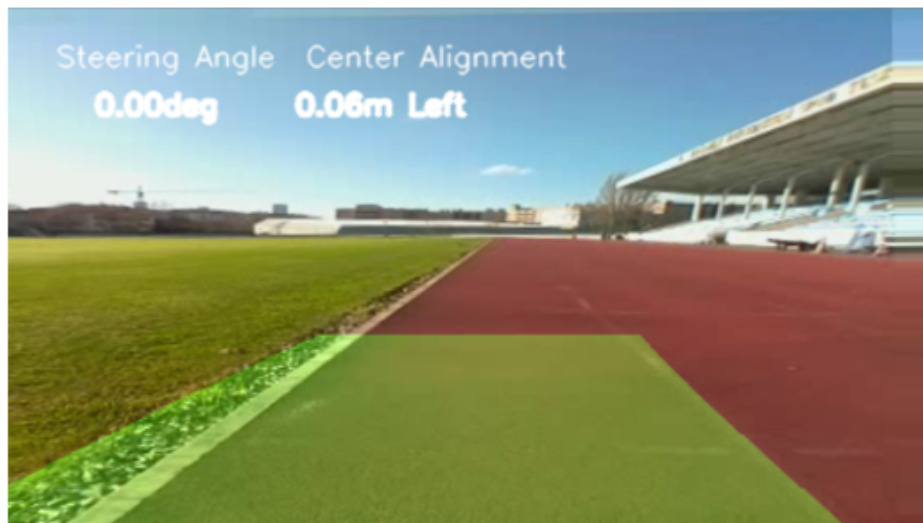
Table 4.1. Success rate of all video records.

	Clockwise		Counter-Clockwise	
	5.5 km/h	6.6 km/h	5.5 km/h	6.6 km/h
Lane-1	95.3 %	91.2 %	87.5 %	78.4 %
Lane-3	90.0 %	89.7 %	82.8 %	74.3 %
Lane-5	86.2 %	82.2 %	87.7 %	89.9 %

The video records for different lanes, direction and speeds were captured and analyzed in order to understand robustness of the lane detection algorithm. All results are shown in Table 4.1. There are some difference between results. One factor for this performance variability was the running speed. High speed running may have caused high vibration for the camera. Although the algorithm had an image stabilization function, a certain level of vibration might cause performance degradation. Another



(a)



(b)

Figure 4.1. Lane detection results. a)Turning part of track, b) Straight part of track.

obvious performance difference factor was the running direction. As can be seen in Table 4.1, algorithm performance for clockwise running was more successful than the counter clockwise running. This might be due to the difference in illumination and shadow factor in the open space. One of the other reason for the performance decrease in the algorithm might be related to the perspective transform of each frame. Transformation matrix was calculated only for the straight section of the running track, so frame transformation in the turning region caused erroneous results. Finally, some problems were related to physical condition of the running track. In some parts of the track, the lane lines had been severely erased and these regions affected the overall performance of the algorithm. Mechanical revisions for vibration isolation of the prototype and physical condition of the running track may increased the performance of the lane detection algorithm. Other than the physical problems, color and gradient filters of the algorithm could be tuned to overcome the illumination and shadow effects. Finally, using different transformation matrix in different regions might minimize the problems caused by perspective transform.

4.1.2. Steering Angle Calculation Performance

The steering angle was calculated with the second degrees polynomials for the detected lanes. The calculated steering angles were compared with desired steering angles for every seconds. The desired steering angle should be 0 at the straight part of the track, and increases steadily from 0 degrees to 45 degrees in the first quarter of the turning zone. It drops from 45 degrees to 0 degrees in the second quarter, and the user should reach the middle of the turning zone. The same steering angle pattern was used within the 3rd and 4th quadrants of the turning zone. The steering angle comparison of all records are given in figs. 4.2 to 4.13

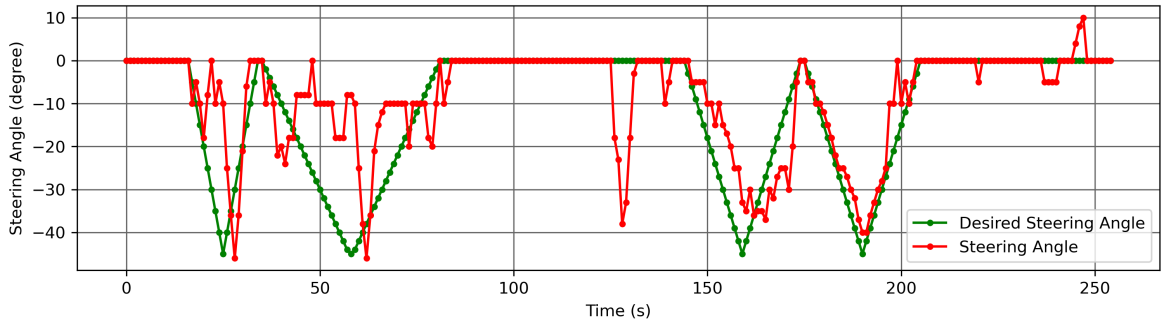


Figure 4.2. Steering angle results (Lane-1-CCW-5.5 km/h) vs desired steering angles.

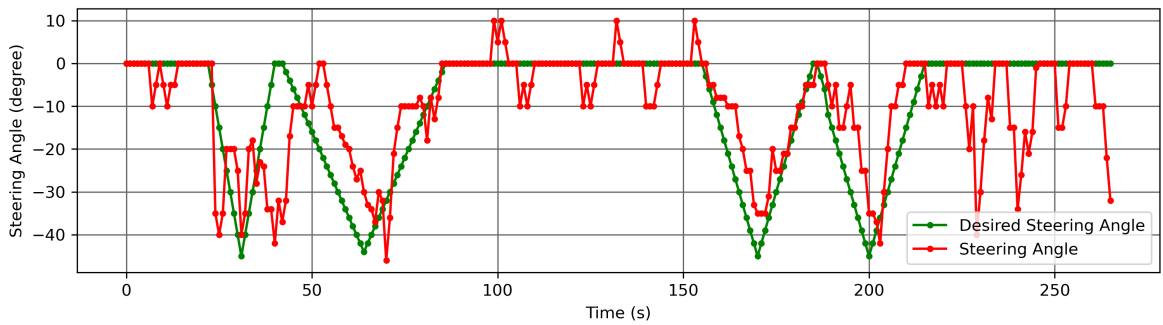


Figure 4.3. Steering angle results (Lane-3-CCW-5.5 km/h) vs desired steering angles.

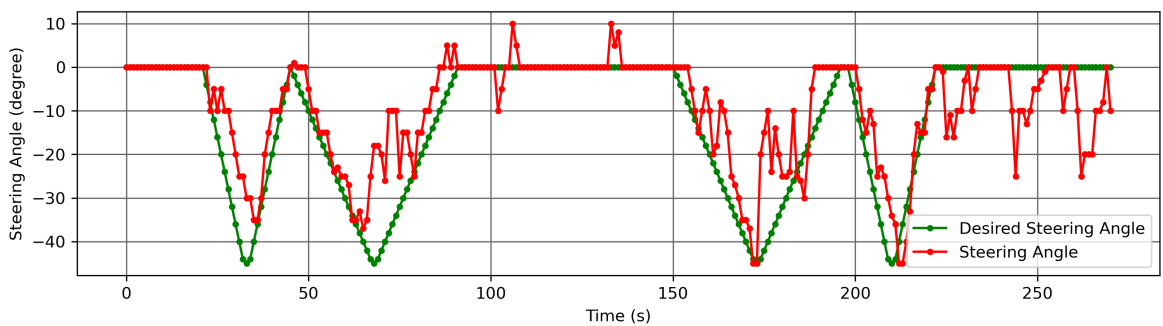


Figure 4.4. Steering angle results (Lane-5-CCW-5.5 km/h) vs desired steering angles.

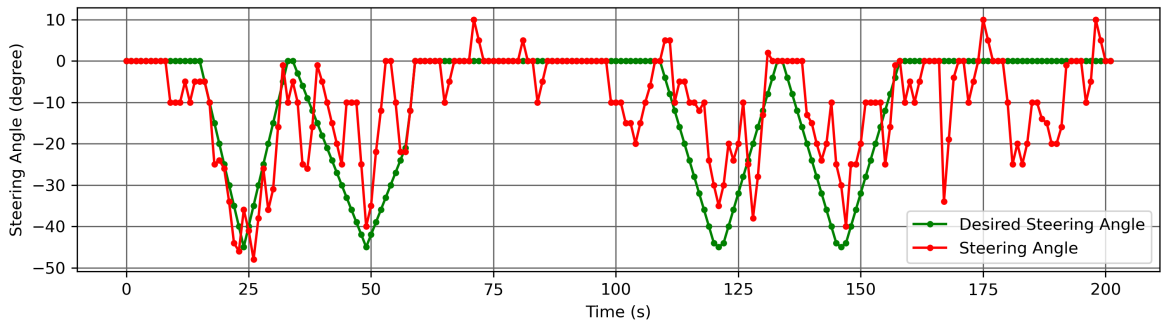


Figure 4.5. Steering angle results (Lane-1-CCW-6.6 km/h) vs desired steering angles.

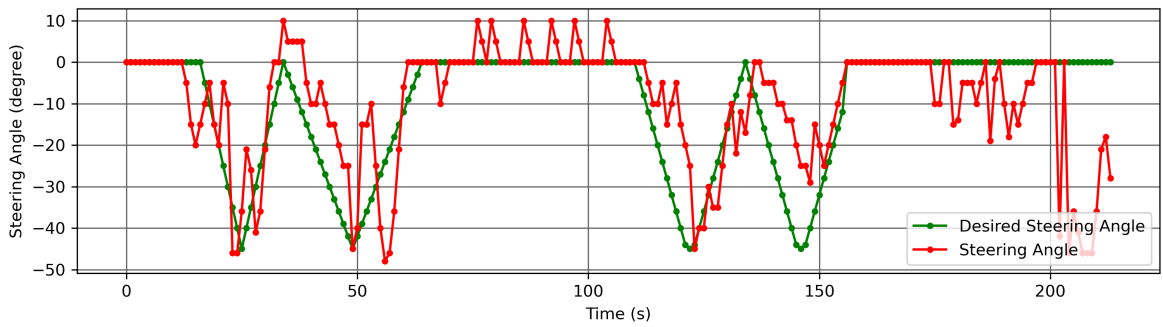


Figure 4.6. Steering angle results (Lane-3-CCW-6.6 km/h) vs desired steering angles.

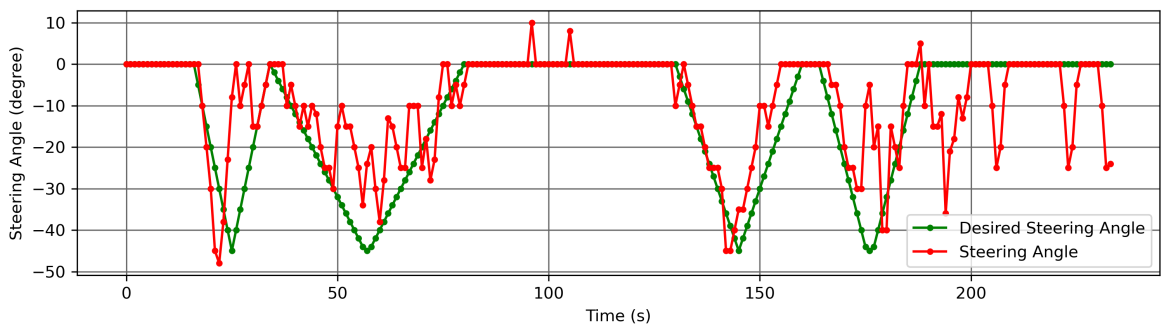


Figure 4.7. Steering angle results (Lane-5-CCW-6.6 km/h) vs desired steering angles.

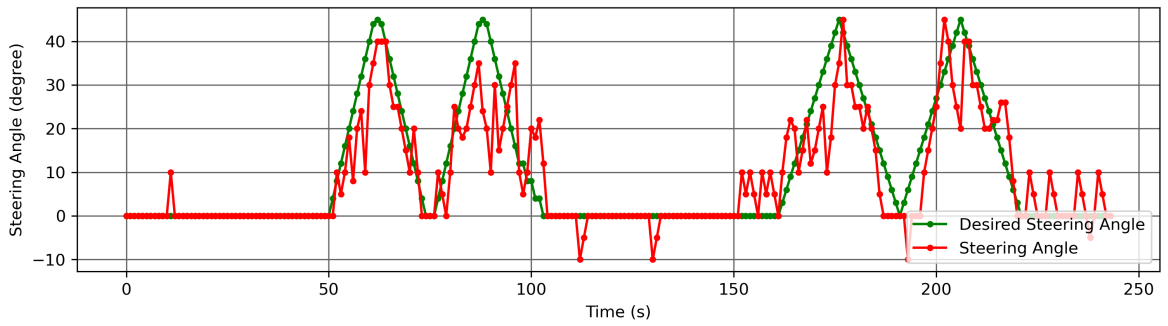


Figure 4.8. Steering angle results (Lane-1-CW-5.5 km/h) vs desired steering angles.

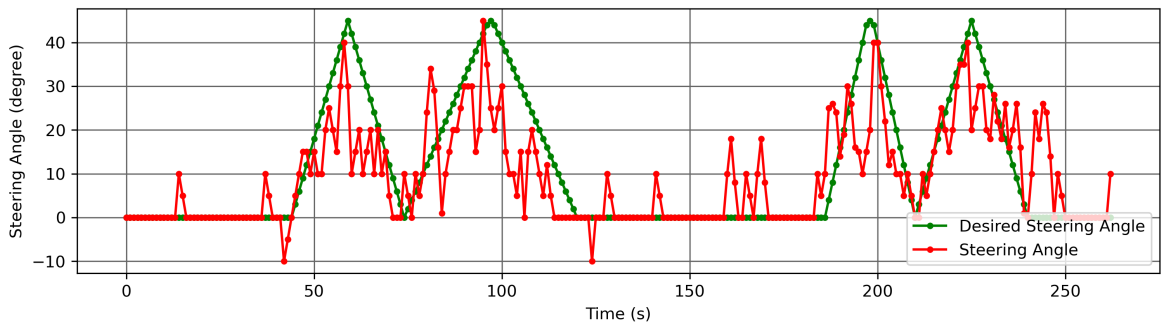


Figure 4.9. Steering angle results (Lane-3-CW-5.5 km/h) vs desired steering angles.

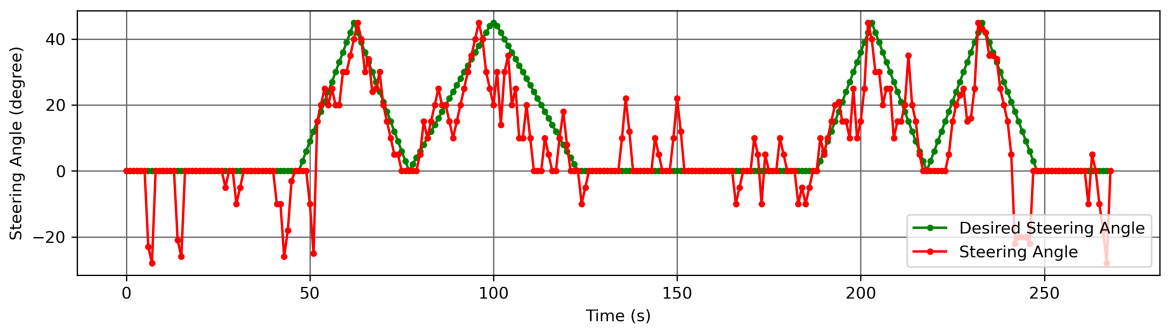


Figure 4.10. Steering angle results (Lane-5-CW-5.5 km/h) vs desired steering angles.

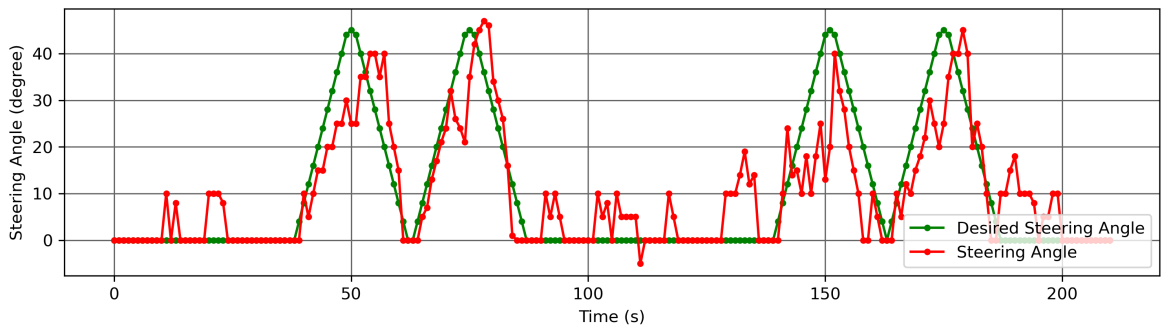


Figure 4.11. Steering angle results (Lane-1-CW-6.6 km/h) vs desired steering angles.

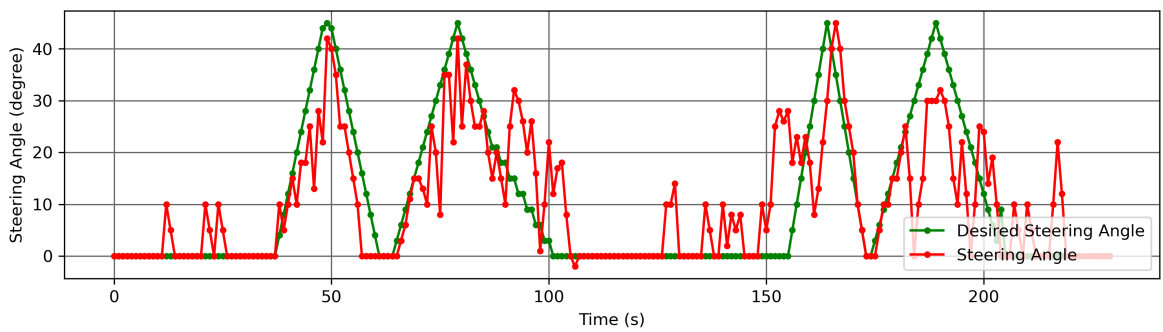


Figure 4.12. Steering angle results (Lane-3-CW-6.6 km/h) vs desired steering angles.

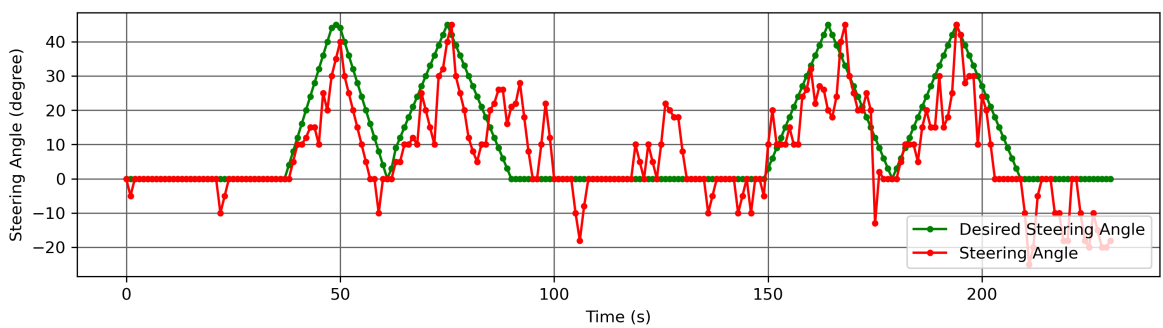


Figure 4.13. Steering angle results (Lane-5-CW-6.6 km/h) vs desired steering angles.

As can be seen in these figures, the desired steering angles and the calculated angles are mostly matched. True turning direction was the critical part of the visually impaired navigation. The calculated steering angles were the same as the desired steering angles in terms of the direction. That means algorithm can find true direction of the lanes. However, there were some noisy calculated angles in the straight part of the track, and there was no complete match in turning parts of the lanes. The root-mean-square-error (RMSE) of the all running records are shown in Table 4.2. Most of these errors were due to the erroneous results coming from the lane detection algorithm which were related to the vibration of the camera, physical condition of the field, illumination and shadow effects.

Table 4.2. Root mean square errors (RMSE) of the calculated steering angles for all running records.

	Clockwise		Counter-Clockwise	
	5.5 km/h	6.6 km/h	5.5 km/h	6.6 km/h
Lane-1	7.3°	8.4°	10.2°	11.1°
Lane-3	9.7°	9.2°	10.9°	13.3°
Lane-5	10.1°	10.4°	8.9°	10.7°

4.2. Haptic Feedback Performance of System

In this section, test results of the skin stretch feedback system are given and overall performance of the wearable prototype is discussed. All tests are completed with three able-bodied subjects.

4.2.1. Static Test Results

The sample steering angles were created at 15 degree intervals from -45 (most-left) to +45 (most-right) and sent the subject randomly. One test consists of 20 random steering angles in total. Prediction accuracy table of static tests for all subjects is given in Table 4.3. Before each static test, a training session was applied users to get familiar

with the general working logic of the feedback. The better prediction accuracies in the second test clearly indicated that the use of the device can be learned quickly. Mean prediction accuracy of the second test was 88.3 %.

Table 4.3. Static test prediction accuracies of all subjects .

	Accuracy %			
	Subject #1	Subject #2	Subject #3	Mean
Test-1	50 %	55 %	60 %	55 %
Test-2	95 %	85 %	85 %	88.3 %

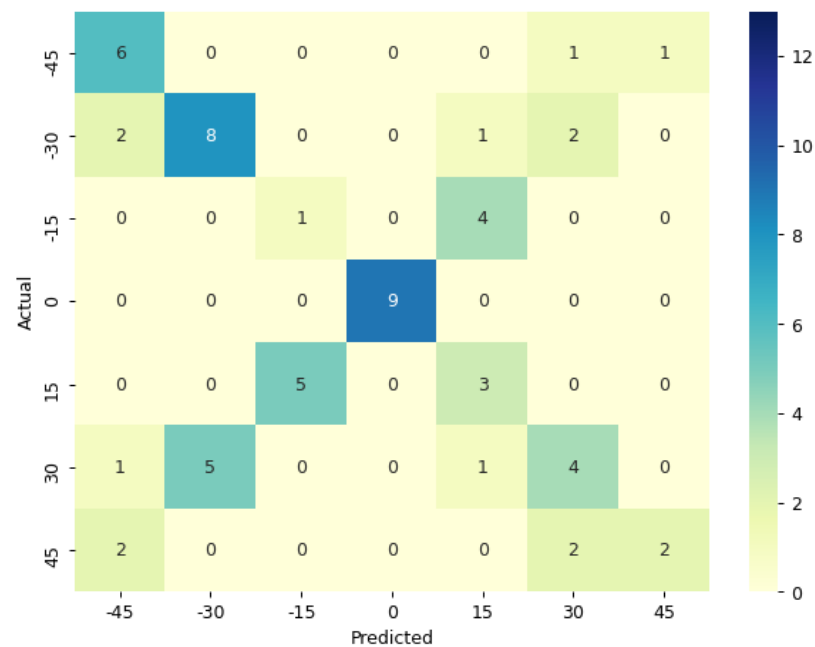


Figure 4.14. Confusion matrix of Test-1.

In order to get deeper understanding of the error source, confusion matrix of the first test is shown in Figure 4.14. The most successfully predicted steering angle was 0 degree among all the random feedback. The least accurate predictions were made for -15 degree steering angle and subjects were able to predict this feedback with only 20 % accuracy for the first static test. Subjects responded to this feedback as +15 degree with a rate of 80 %.

Based on this result, it has been observed that 70.4 % of the total errors were caused only by the wrong direction estimation. In addition, only 18.5 % of the total errors were related to incorrect estimation of the level of the feedback. The meaning of these results is that while subjects can easily distinguish feedback levels, they can be confused in predicting the feedback directions.

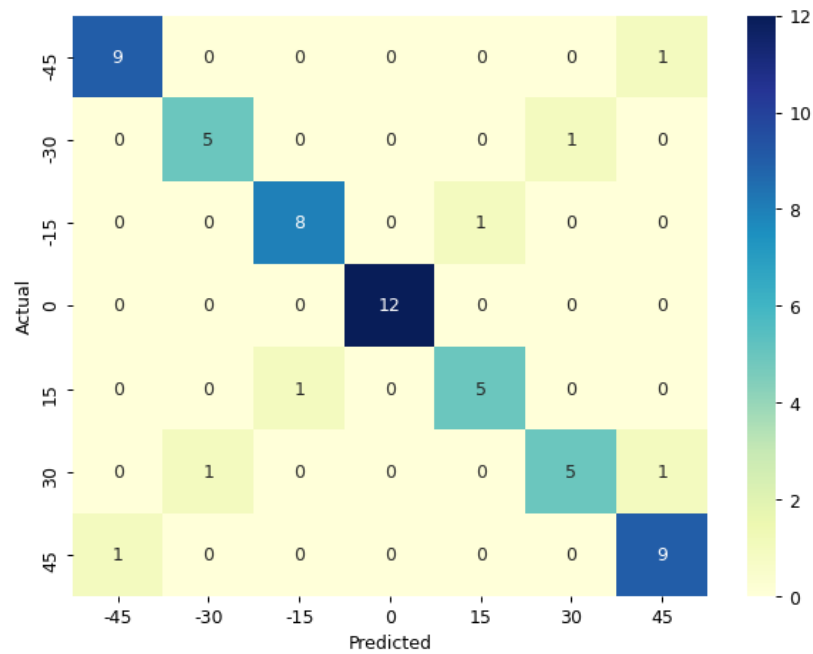


Figure 4.15. Confusion matrix of Test-2.

In order to overcome this confusion, more training sessions were applied to subjects before the second test. Confusion matrix of the second test is shown in Figure 4.15. The total error rate for the second test was only 11.6 % and 85.7 % of these errors were only due to confusion in the direction of the feedback. However, the serious decrease in the total number of errors indicated that the users got used to the device more, and training sessions were helpful to understand the working principle of the device. The cornerstone of these results is the intuitional capacity of the prototype.

4.2.2. Pre-recorded Test Results

Two different videos were prepared from the previously recorded videos which were used at the algorithm performance tests, and used in this test. All predictions of three subjects were compared with the desired steering angles. Figure 4.16 and 4.17 show these comparison results. As can be seen in these figures, exact match between the prediction and desired values were not observed. However, subjects might be able to discriminate direction of the feedback. Subject 1 and 2 were more sensitive to all feedback and changed their prediction immediately, but this sensitivity may have caused a confusion in some parts of the tests. Therefore, their RMSE's were higher than Subject-3 for both tests. All RMSE results are given in Table 4.4. The first and the second tests were conducted consecutively on the same day, and the results of the 1st and 3rd users show that the success rates increase as the user gets used to the prototype.

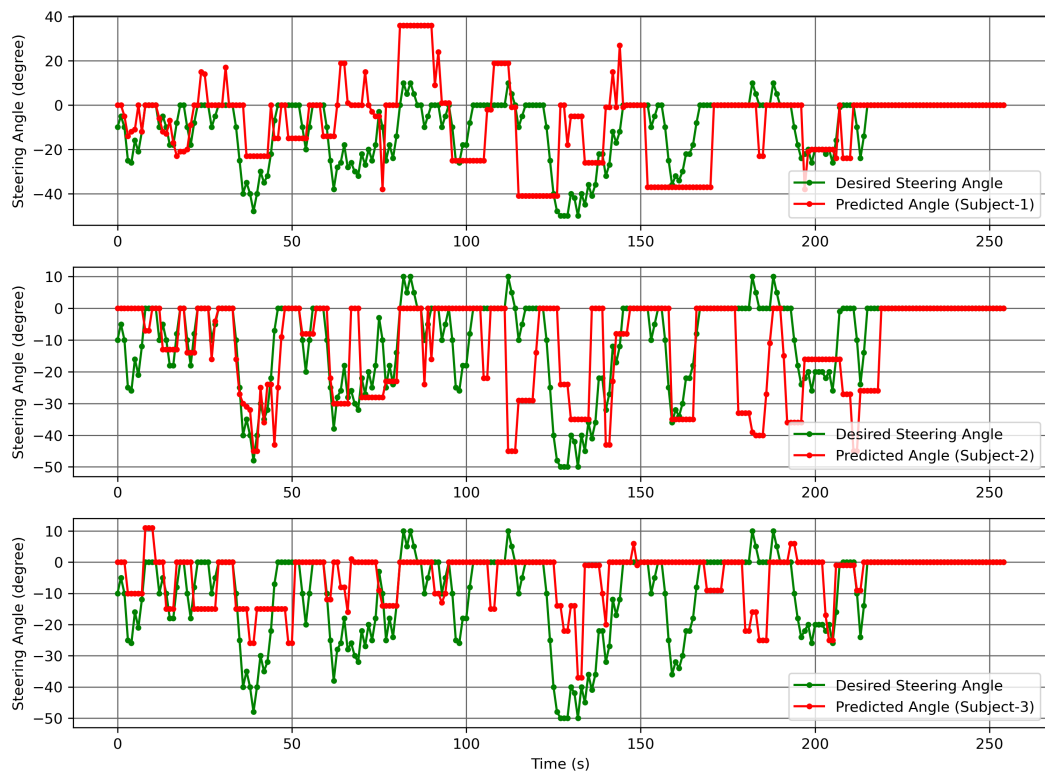


Figure 4.16. First pre-recorded test steering angle comparison.

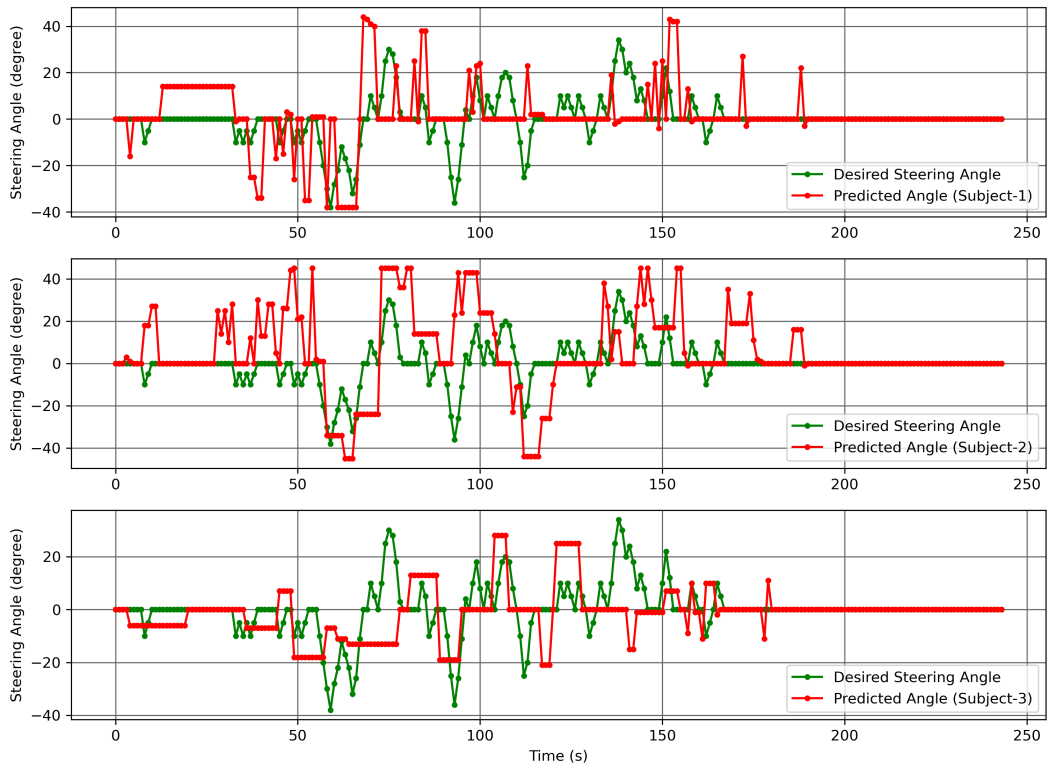


Figure 4.17. Second pre-recorded test steering angle comparison.

Table 4.4. RMSE of first and second pre-recorded tests.

	RMSE		
	Subject-1	Subject-2	Subject-3
Test-1	18.9°	15.8°	14.4°
Test-2	13.9°	18.6°	11.5°

4.2.3. Real-time Test Results

Usability of the prototype in real world environment was evaluated with 3 different subjects. All users test the prototype for one complete lap which is around 400 meters. In case of any emergency situation, all subjects completed the run with the test coordinator. The prototype continued to operate fully functional throughout the entire experiments. Total time of the run, total number of lane departures and audible directional warnings were noted by the test coordinator during the real-time test. Results of all subjects are given in Table 4.5.



Figure 4.18. Preparation and implementation phase of the real-time test.

The most successful results belong to the Subject-1. This participant changed lanes only once within 400 meters and was warned only 4 times in total. This user is interested in running as an amateur and completed the training for the static tests on the same day before the real-time test. However, other users' error numbers and completion times for one lap were not as good as the first subject. The reason why the results were so different might be related to the static test training timing and sports background of the user. The second and third subjects, who are not as interested in running as the first user, completed their static test training a few days before the pre-recorded test. The results of the static test and the real-time test show that the efficiency of the use of the device is directly related to the experience and training.

Table 4.5. Real-time test results of all subjects .

	Lane Violations	Directional Warnings	Time of the run (s)
Subject-1	1	4	260
Subject-2	9	24	369
Subject-3	12	21	417

After all tests, the users filled out a questionnaire in which they evaluated the overall performance, intuitiveness, usability and ergonomics of the device. Questions were scored between 1 and 5. 1 point means strongly agree and 5 point means strongly disagree. Table 4.6 shows the average scores of all questions.

Table 4.6. Questionnaire results.

	Average Results (1-5)
Feedback mechanism is easy to understand	4.3
Static and pre-recorded tests are easy	4.3
Real-time test is easy	3
Not feel any discomfort from the device	4
Easy to wear and ergonomic	3.7
Feedback are understandable and effective	4
Feedback are intuitive	3.7
Device usage required a high concentration	3.7
Useful for visually impaired	4.7

5. CONCLUSION

In this study, a novel wearable assistive device for visually impaired runners has been designed, developed and tested. There are many studies and devices in the literature and in the market for the guidance of the visually impaired persons. However, there are very few studies targeting visually impaired persons who do sports, and the feedback systems of these studies are solely on vibration and sound. In this thesis, we proposed that a device which uses skin stretch feedback is more suitable and intuitive for such a task. This proposed device was based on image processing algorithm to detect lanes and calculate steering angles. After analyzing performance of the designed prototype with algorithm and physical feedback tests, the algorithm can detect lanes with the mean success rate of 86.5 % and average RMSE of all steering calculation was found as 10.1°. As a result of external disturbances such as vibration and deformation of the running track, the algorithm performance decreased at high speed running and in areas where the lane lines were not clear. Subjects predicted correct direction and magnitude of feedback with the mean accuracy of 88.3 % according to the static test results and mean RMSE for real-time test is 15.6°. All subjects also completed the real-time test without getting into a dangerous situation. In general, the results show that, the learnability of the device is high, and the user's performance increases significantly with experience. According to the questionnaire, the skin stretch feedback and the overall prototype were found intuitive, understandable, effective, ergonomic and most importantly useful for visually impaired.

5.1. Contributions and Originality

The novel feedback system and the targeted user group constitute the originality of this study. The main difference of the designed wearable assistive device compared to other devices in the literature is skin stretch feedback mechanism. This mechanism provides intuitive and accurate feedback to the user. Another novelty of the prototype is related to the target group. There are very few studies for visually impaired runners

in the literature [2, 5–7], however, our study is completely different than these studies in terms of feedback mechanism and ergonomics.

This study will contribute to the literature as a conference paper. The findings of the study and design details will be submitted to IEEE World Haptics Conference 2021.

5.2. Future Work

The designed system has been tested on able-bodied users so far. In order to make the system more robust, the lane detection algorithm and mechanical issues could be improved. In some cases, our device is severely affected by camera vibration. Active or passive vibration damping system will be added to the prototype to reduce the vibration effect. In addition to that, deep learning models for lane detection might be implemented in order to solve classical illumination variability problem of color and gradient filters. Apart from these, an obstacle detection and warning algorithm that can detect possible obstacles and other runners in the same lane will be developed and added to the system. Finally, the complete prototype might be tested with actual target group.

REFERENCES

1. “Blindness and Vision Impairment”, <https://www.who.int/news-room/fact-sheets/detail/blindness-and-visual-impairment>, visited on 20.09.2020.
2. Peiris, H., C. Kulasekara, H. Wijesinghe, B. Kothalawala, N. Walgampaya and D. Kasthurirathna, “EyeVista: An Assistive Wearable Device for Visually Impaired Sprint Athletes”, *2016 IEEE International Conference on Information and Automation for Sustainability (ICIAfS)*, pp. 1–6, 2016.
3. Mancini, A., E. Frontoni and P. Zingaretti, “Mechatronic System to Help Visually Impaired Users During Walking and Running”, *IEEE Transactions on Intelligent Transportation Systems*, Vol. 19, pp. 649–660, 2018.
4. “Convention on the Rights of Persons with Disabilities”, <https://www.ohchr.org/EN/HRBodies/CRPD/Pages/ConventionRightsPersonsWithDisabilities.aspx47>, visited on 20.09.2020.
5. C.Ramer, C.Ziegler, S. Reitelshöfer and J. Franke, “Sensor-guided jogging for visually impaired”, *5th IEEE RAS EMBS International Conference on Biomedical Robotics and Biomechatronics (BioRob)*, pp. 467–472, 2014.
6. C.Ramer, T. Lichtenegger, J. Sessner, M. Landgraf and J. Franke, “An adaptive, color based lane detection of a wearable jogging navigation system for visually impaired on less structured paths”, *6th IEEE RAS EMBS International Conference on Biomedical Robotics and Biomechatronics (BioRob)*, pp. 741–746, 2016.
7. Skripko, A., P. Skripko, A. Gailitis and L. Selavo, “RF-based node system for blind navigation in running activities”, *2008 International Conference on Signals and Electronic Systems*, pp. 527–530, 2008.
8. Taşkın, C., E. Aslan and E. Yiğitbaşı, “Boğaziçi University Bachelor Thesis -

- Navigation Aid for Visually Impaired Runners”, pp. 1–59, 2018.
9. Bark, K., J. W. Wheeler, S. Premakumar and M. R. Cutkosky, “Comparison of Skin Stretch and Vibrotactile Stimulation for Feedback of Proprioceptive Information”, *2008 Symposium on Haptic Interfaces for Virtual Environment and Teleoperator Systems*, pp. 71–78, 2008.
 10. Gallo, S., D. Chapuis, L. Santos-Carreras, Y. Kim, P. Retornaz, H. Bleuler and R. Gassert, “Augmented White Cane with Multimodal Haptic Feedback”, *International Conference on Biomedical Robotics and Biomechatronics*, pp. 149–155, 2010.
 11. “SmartCane Device”, <http://assistech.iitd.ernet.in/smartcane.php>, visited on 21.09.2020.
 12. Cosgun, A., E. A. Sisbot and H. I. Christensen, “Evaluation of rotational and directional vibration patterns on a tactile belt for guiding visually impaired people”, *IEEE Haptics Symposium 2014*, pp. 367–370, 2014.
 13. Velázquez, R., E. Pissaloux and A. Lay-Ekuakille, “Tactile-Foot Stimulation Can Assist the Navigation of People with Visual Impairment”, *Applied Bionics and Biomechanics*, p. 9, 2015.
 14. Scheggi, S., A. Talarico and D. Prattichizzo, “A remote guidance system for blind and visually impaired people via vibrotactile haptic feedback”, *22nd Mediterranean Conference on Control and Automation*, pp. 20–23, 2014.
 15. Bark, K., J. Wheeler, G. Lee, J. Savall and M. Cutkosky, “A wearable skin stretch device for haptic feedback”, *World Haptics 2009 - Third Joint EuroHaptics conference and Symposium on Haptic Interfaces for Virtual Environment and Teleoperator Systems*, pp. 464–469, 2009.
 16. Battaglia, E., J. P. Clark, M. Bianchi, M. G. Catalano, A. Bicchi and M. K.

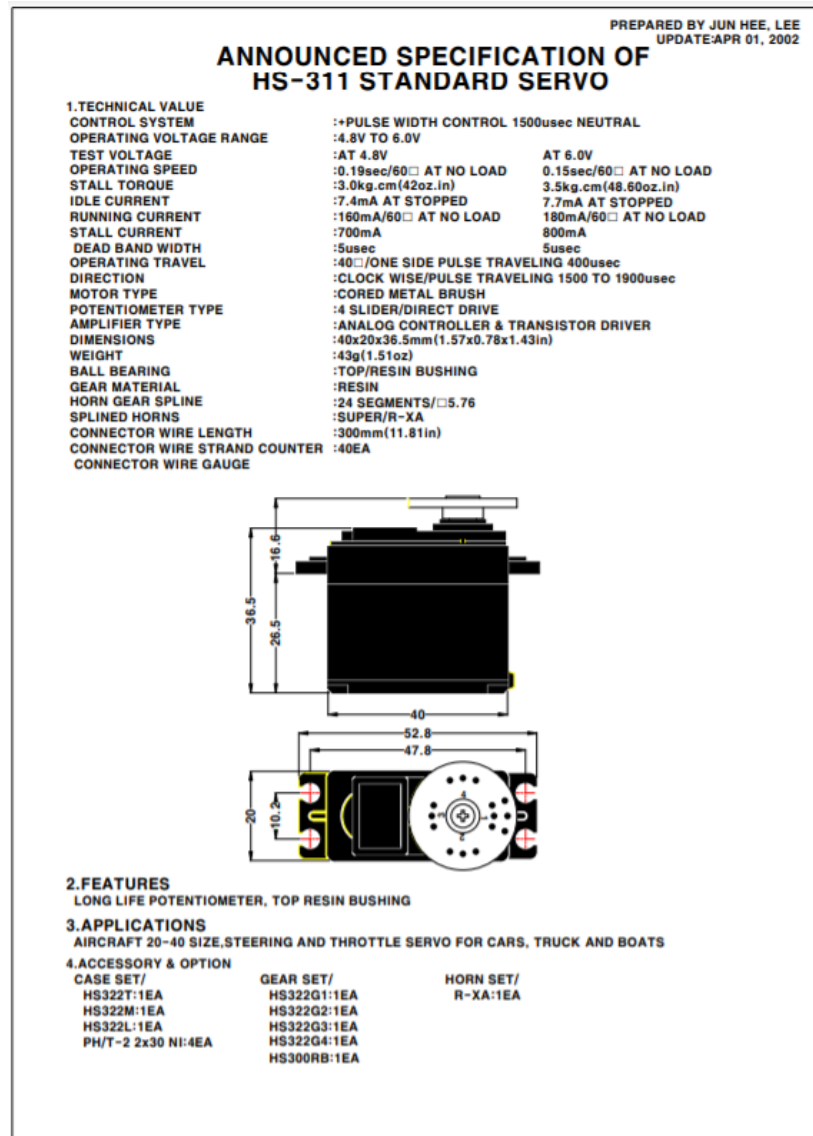
- O'Malley, "The Rice Haptic Rocker: Skin stretch haptic feedback with the Pisa/IIT SoftHand", *2017 IEEE World Haptics Conference (WHC)*, pp. 7–12, 2017.
17. Kayhan, O., A. K. Nennioglu and E. Samur, "A skin stretch tactor for sensory substitution of wrist proprioception", *2018 IEEE Haptics Symposium (HAPTICS)*, pp. 26–31, 2018.
 18. Chossat, J.-B., D. K. Y. Chen, Y.-L. Park and P. B. Shull, "Soft Wearable Skin-Stretch Device for Haptic Feedback Using Twisted and Coiled Polymer Actuators", *IEEE Transactions on Haptics*, Vol. 12, pp. 521–532, 2019.
 19. B.B.Edin and N.Johansson, "Skin strain patterns provide kinaesthetic information to the human central nervous system", *The Journal of Physiology*, Vol. 487,1, pp. 243–251, 1995.
 20. B.B.Edin, "Quantitative Analyses of Dynamic Strain Sensitivity in Human Skin Mechanoreceptors", *Journal of Neurophysiology*, Vol. 92, pp. 3233–3243, 2005.
 21. Kumar, K., B. Champaty, U. K., R. Chachan and K. Pal, "Development of an Ultrasonic Cane as a Navigation Aid for the Blind People", *2014 International Conference on Control, Instrumentation, Communication and Computational Technologies (ICCICCT)*, pp. 475–479, 2014.
 22. Saaaid, M., A. Mohammad and M. M. Ali, "Smart cane with range notification for blind people", *2016 IEEE International Conference on Automatic Control and Intelligent Systems (I2CACIS)*, pp. 225–229, 2016.
 23. Wang, Y. and K. J. Kuchenbecker, "HALO: Haptic Alerts for Low-hanging Obstacles in White Cane Navigation", *Departmental Papers (MEAM), University of Pennsylvania*, pp. 527–532, 2012.
 24. Agrawal, M. P. and A. R. Gupta, "Smart Stick for the Blind and Visually Impaired People", *2018 Second International Conference on Inventive Communication and*

- Computational Technologies (ICICCT)*, pp. 542–545, 2018.
25. Meshram, V. V., K. Patil, V. A. Meshram and F. C. Shu, “An Astute Assistive Device for Mobility and Object Recognition for Visually Impaired People”, *IEEE Transactions on Human-Machine Systems*, Vol. 49, pp. 449–460, 2019.
 26. Takizawa, H., S. Yamaguchi, M. Aoyagi, N. Ezaki and S. Mizuno, “Kinect cane: an assistive system for the visually impaired based on the concept of object recognition aid”, *Personal and Ubiquitous Computing*, Vol. 19, pp. 955–965, 2015.
 27. Mancini, A., E. Frontoni and P. Zingaretti, “Embedded Multisensor System for Safe Point-to-Point Navigation of Impaired Users”, *IEEE Transactions on Intelligent Transportation Systems*, Vol. 16, pp. 3543–3555, 2015.
 28. Kanwal, N., E. Bostanci, K. Currie and A. F. Clark, “A Navigation System for the Visually Impaired: A Fusion of Vision and Depth Sensor”, *Applied Bionics and Biomechanics 2015*, p. 16, 2015.
 29. Bai, J., Z. Liu, Y. Lin, Y. Li, S. Lian and D. Liu, “Wearable Travel Aid for Environment Perception and Navigation of Visually Impaired People”, *MDPI Electronics*, p. 697, 2019.
 30. Aladrén, A., G. López-Nicolás, L. Puig and J. J. Guerrero, “Navigation Assistance for the Visually Impaired Using RGB-D Sensor With Range Expansion”, *IEEE Systems Journal*, Vol. 10, pp. 922–932, 2016.
 31. Lin, Y., K. Wang, W. Yi and S. Lian, “Deep Learning based Wearable Assistive System for Visually Impaired People”, *CloudMinds Technologies Inc*, pp. 2549–2557, 2019.
 32. Vlaminck, M., H. Luong, H. V. Nam, H. Vu, P. Veelaert and W. Philips, “Indoor assistance for visually impaired people using a RGB-D camera”, *IEEE Southwest Symposium on Image Analysis and Interpretation*, pp. 161–164, 2016.

33. Kamal, A., P. N. Indi, S. Banerjee, A. R. Pardasani and V. Garg, “Smart Assistive Navigation Devices for Visually Impaired People”, *2019 IEEE 4th International Conference on Computer and Communication Systems (ICCCS)*, pp. 725–729, 2019.
34. Priya, C., C. Ramya, S. Dhanasekar, S. R. V. S and Y. G, “Aiding Navigation for Visually Impaired Persons”, *Test Engineering and Management*, pp. 10985–10988, 2020.
35. Kumar, A., R. Patra, . Mukhopadhyay and A. K. Majumdar, “An Electronic Travel Aid for Navigation of Visually Impaired Persons”, *Communication Systems and Networks (COMSNETS)*, Vol. 82, pp. 10985–10988, 2011.
36. Schwarze, T., M. Lauer, M. Schwaab, M. Romanovas, S. Bohm and T. J. [U+FFFF] urgensohn, “An Intuitive Mobility Aid for Visually Impaired People based on Stereo Vision”, *2015 IEEE International Conference on Computer Vision Workshop (ICCVW)*, pp. 409–417, 2015.
37. Kotyan, S., P. K. Sahu, N. Kumar and V. U, “Drishtikon: An advanced navigational aid system for visually impaired people”, *2018 Conference on Information and Communication Technology (CICT)*, pp. 1–6, 2019.
38. Zhang, X., X. Yao, Y. Zhu and F. Hu, “An ARCore Based User Centric Assistive Navigation System for Visually Impaired People”, *MDPI Applied Sciences*, Vol. 9, p. 989, 2019.
39. Kiuru, T., M. Metso, M. Utriainen, K. Metsävainio, H.-M. Jauhonen, R. Rajala, R. Savenius, M. Ström, T.-N. Jylhä, R. Juntunen and J. Sylberg, “Assistive device for orientation and mobility of the visually impaired based on millimeter wave radar technology—Clinical investigation results”, *Cogent Engineering*, pp. 1–5, 2018.
40. van Erp, J. B. F., L. C. M. Kroon, T. Mioch and K. I. Paul, “Obstacle Detection

- Display for Visually Impaired: Coding of Direction, Distance, and Height on a Vibrotactile Waist Band”, *Frontiers in ICT*, p. 23, 2017.
41. Katzschmann, R. K., B. Araki and D. Rus, “Safe Local Navigation for Visually Impaired Users With a Time-of-Flight and Haptic Feedback Device”, *IEEE Transactions on Neural Systems and Rehabilitation Engineering*, Vol. 26, pp. 583–593, 2018.
 42. Pallejà, T., M. Tresanchez, M. Teixidó and J. Palacin, “Bioinspired Electronic White Cane Implementation Based on a LIDAR, a Tri-Axial Accelerometer and a Tactile Belt”, *MDPI Sensor (Basel)*, Vol. 10, pp. 11322—11339, 2010.
 43. Kon, Y., T. Nakamura, M. Sato and H. Kajimoto, “Effect of Hanger Reflex on walking”, *2016 IEEE Haptics Symposium (HAPTICS)*, pp. 313–318, 2016.
 44. Bourne, M., “Radius of Curvature”, <https://www.intmath.com/applications-differentiation/8-radius-curvature.php>, visited on 11.10.2020.
 45. Bark, K. Y. J., *Stanford University Doctor of Philosophy Thesis - Rotational Skin Stretch Feedback: A New Approach to Wearable Haptic Display*, 2009, <http://bdml.stanford.edu/twiki/pub/Haptics/SkinStretch/ThesisSingleSideColor.pdf>, March 2009.

APPENDIX A: DATASHEET



HITEC RCD KOREA INC.

Figure A.1. Servo motor datasheet.